An examination of the process and magnitude of ionospheric plasma supply to the magnetosphere.

M. Huddleston, C.R. Chappell, Dominique C. Delcourt, T.E. Moore, B.L. Giles, M.O. Chandler

An examination of the process and magnitude of ionospheric plasma supply to the magnetosphere

M. M. Huddleston,[1,2] C. R. Chappell,[1] D. C. Delcourt,[3] T. E. Moore,[4] B. L. Giles,[4] and M. O. Chandler[5]

Received 23 January 2004; revised 9 August 2005; accepted 12 September 2005; published 3 December 2005.

[1] The contribution of ionospheric plasma to the Earth's magnetosphere has been recognized for more than 3 decades. The magnitude of this contribution has become more evident over that same time period with the observed magnitude of the low-energy ionospheric supply increasing as the measurement techniques improved. Estimates based on Dynamics Explorer measurements in the mid-1980s suggested that the ionospheric plasma supply is sufficient to populate the plasmasphere, plasma trough, plasma sheet, and magnetotail lobes. Recent measurements from the Thermal Ion Dynamics Experiment on the Polar spacecraft have been used in conjunction with an ion trajectory model to reexamine the process and magnitude of the ionospheric supply of magnetospheric plasma. These measurements reveal the energy, pitch angle, and flux characteristics of the upward flowing polar wind over broad regions of the high-latitude ionosphere. Onboard measurement of spacecraft potential is found to be a fundamental element in interpreting the measured ion outflow. Newly derived polar wind fluxes are determined to be near 6.0×10^7 ions cm^{-2} s^{-1} at 5000 km altitude during local winter and magnetically quiet conditions. Using the measured ionospheric source characteristics in combination with the trajectory code reveals the nature of the ionospheric/magnetosphere filling process and shows that the ionospheric source is sufficient to supply the observed densities and energies of the plasma sheet and magnetotail lobes. Many of the ionospheric particles are further transformed to ring current energies and locations after circulation through the plasma sheet. This measurement/calculation approach is able to show which regions of the high-latitude ionosphere are important for plasma sheet/ring current filling. The ionospheric sources used in the calculations include the dominant polar wind, the cleft ion fountain, and the auroral zone.

Citation: Huddleston, M. M., C. R. Chappell, D. C. Delcourt, T. E. Moore, B. L. Giles, and M. O. Chandler (2005), An examination of the process and magnitude of ionospheric plasma supply to the magnetosphere, *J. Geophys. Res.*, *110*, A12202, doi:10.1029/2004JA010401.

1. Objectives

[2] Among the numerous unresolved issues in magnetospheric physics, the question of plasma origins is perhaps the most fundamental. Yet after decades of research, a number of important questions regarding the exact source strength of the ionosphere remain unanswered [*Hultqvist*, 1982; *Yau and Andre*, 1997; *Chappell et al.*, 2000]. Without this knowledge of plasma origins, it is impossible to accurately model the characteristics and dynamics of the magnetosphere or upper ionosphere. Although some have argued for the ionosphere as a major supplier of magnetospheric plasma [*Chappell et al.*, 1987], many others have concluded that the solar wind must somehow enter into the magnetosphere to provide a substantial supply of energetic ions to the plasma sheet [*Eastman et al.*, 1985; *Kivelson and Spence*, 1988; *Lennartsson*, 2001]. A solar wind source alone, however, is incapable of explaining the levels of O^+ within the plasma sheet and ring current [*Shelley et al.*, 1972]. The extraction of heavy oxygen ions from the ionosphere suggests that lighter terrestrial H^+ could be "hiding" in the magnetosphere as well, indistinguishable from protons of solar wind origin [*Seki et al.*, 2003].

[3] If the ionosphere is in fact a major source for magnetospheric plasma, the question then remains as to how cold dense ionospheric ions are energized and transported out to become the hot tenuous plasma of the magnetosphere. Single step parallel acceleration models (i.e., ion acceleration through parallel potential drops) have been unable to place enough heavy ions into the magnetosphere to account for observations [*Arnoldy*, 1993]. Al-

[1]Vanderbilt University, Nashville, Tennessee, USA.
[2]Also at Harpeth Hall School, Nashville, Tennessee, USA.
[3]Centre d'etude des Environnements Terrestre et Planétaires, Observatoire de Saint-Maur, St. Maur, France.
[4]NASA Goddard Space Flight Center, Greenbelt, Maryland, USA.
[5]NASA Marshal Space Flight Center, Huntsville, Alabama, USA.

0148-0227/05/2004JA010401

though transverse acceleration (acceleration perpendicular to the local magnetic field) is believed to be an important mechanism behind the generation of low-energy superthermal "upwelling" ions observed in the cusp/cleft region [*Moore et al.*, 1986] as well as low-energy polar wind observed over the polar caps [*Ganguli*, 1996], this mechanism involves complex wave particle interactions that are difficult to model and cannot easily energize ions up to the kilovolt range typical of particles in the plasma sheet and ring current. This issue is particularly important because of the significance of the filling and draining of the plasma sheet during space weather magnetic storm phenomena.

2. Methods of Analysis

[4] To address these questions, this paper will focus on two basic objectives: (1) describe how polar wind and other ion outflows are energized and escape to become magnetospheric plasma and (2) by adding up polar wind, auroral, and other ionospheric outflows, estimate the total ionospheric contribution to the magnetosphere (in particular the plasma sheet) under steady state conditions. The combination of data and modeling provide improved outflow estimates while also explaining where the terrestrial ions travel and how they become energized along the way. This information can then be used to quantify the amount of ionospheric plasma that contributes to the energetic plasma sheet as well as other regions within the magnetosphere.

[5] In order to accurately model ionospheric outflows, what is needed is a detailed description of the ion "output" of the ionosphere and, consequently, the terrestrial ion "input" to the magnetosphere. We could think of this data set as the polar wind "source grid" for the magnetosphere. It would contain information about polar wind fluxes, energies, pitch angles, and species, all as a function of location (latitude, local time, and altitude). For this step it is important to note that the focus of this paper will not be on moments of the outflow distribution (temperatures, mach number, densities, etc.) but only on establishing the necessary information to use for the ion trajectory mapping that follows. Newly analyzed data from the Thermal Ion Dynamics Experiment (TIDE) [*Moore et al.*, 1995] on board the Polar satellite have been utilized to provide an improved characterization of the lowest-energy H^+ polar wind outflow. To accurately represent the true polar wind outflow, we must take spacecraft charging into account when calculating fluxes. We have combined the analysis methods of *Su et al.* [1998a] with newly revised onboard spacecraft potential measurements [*Scudder et al.*, 2000] to estimate the polar wind distribution function. This will be an important step that will help to clear up some of the confusion regarding discrepancies between various theory and observation-based flux estimates of the past. Although we do not attempt to perform a detailed comparison with all other polar wind outflow measurements, some basic comparisons are given for context and reference with previous studies.

[6] This new characterization of polar wind H^+ combined with other previously reported ionospheric outflow measurements (detailed below) has provided a comprehensive grid of input parameters to use when modeling what happens to these outflows. A three-dimensional particle tracing code described below will be used to track ions through a steady state model magnetosphere. Given the input parameters of species, energy, pitch angle, and location for the ionospheric source, the model can track each ion noting the changes in energy and pitch angle that occur in various locations. When completed, these ion trajectories give a picture of exactly which outflows travel through which locations in the magnetosphere and how ions are transformed in energy and pitch angle along the way. This information provides an "access map" detailing which populations of ion outflows from which locations can gain access to the magnetotail lobes, plasma sheet, and ring current.

[7] Once the basic link between the ionosphere and the outer magnetosphere (in particular, the plasma sheet) is established, quantitative estimates of the ionospheric plasma contribution can be made. Using the measured fluxes of each ionospheric source (polar wind, cleft ion fountain, and auroral) together with their respective sets of model trajectories, terrestrial ion densities in the tail lobes and plasma sheet can be ascertained. Comparisons can be made determining which ionospheric source locations, ion energies, and pitch angles are most significant in contributing to the plasma sheet and ring current. Finally, a comprehensive total of ionospheric particles entering the plasma sheet will be calculated to conclude whether these terrestrial outflows are sufficient to account for the range of energies and densities reported within the plasma sheet and ring current.

[8] Terrestrial ion outflow is obviously affected by solar wind and magnetospheric conditions, and magnetic substorms may themselves be triggered by the presence of heavy terrestrial ions injected into the plasma sheet [*Cladis and Francis*, 1992; *Daglis and Axford*, 1996; *Moore et al.*, 1999; *Cully et al.*, 2003b]. However, the main purpose here will be to understand the background of terrestrial ion outflow that occurs regardless of magnetospheric conditions. We will also address the general nature of the influence of magnetic activity on ionospheric output but will not deal with individual storm events.

[9] While numerous ionospheric outflow studies have been performed over the years [e.g., *Nagai et al.*, 1983; *Collin et al.*, 1984; *Lockwood et al.*, 1985a; *Cladis*, 1986; *Yau et al.*, 1988; *Kondo et al.*, 1990; *Pollock et al.*, 1990; *Chandler et al.*, 1991; *Yau and Andre*, 1997; *Peterson et al.*, 2001; *Cully et al.*, 2003a], a comprehensive treatment of the very lowest energy component of that outflow has remained difficult. This is primarily due to the phenomenon of spacecraft charging. Any orbiting satellite is exposed to solar ultraviolet photons which constantly bombard its surface. This radiation releases electrons through the photoelectric effect which immediately speed away from the spacecraft. Unless there is a sufficient density of cold electrons present, the spacecraft cannot neutralize itself and thus develops a positive charge that tends to shield any onboard instruments from detecting low-energy positive ions. At altitudes of only a few thousand kilometers, cold electron densities are low enough that spacecraft charging effects become very important. At higher altitudes over the polar caps, spacecraft potentials can reach +40 volts or more [*Scudder et al.*, 2000]. For this reason, even the most rigorous statistics on thermal outflows have been dependent on estimating the spacecraft potential and generally involve fitting a distribution to a Maxwellian or

bi-Maxwellian (e.g., the analysis of *Cully et al.* [2003a], based on the method of *Drakou et al.* [1997]). The uncertainty in the thermal ion outflow measurements is significant since the polar wind has been theorized to be an important source of ionospheric outflow. In this paper we have used data from the TIDE instrument to identify polar wind events. We have compensated for the effects of spacecraft charging by using the filling technique of *Su et al.* [1998a] combined with the spacecraft potential measured simultaneously aboard the Polar satellite [*Harvey et al.*, 1995; *Scudder et al.*, 2000].

3. Statistical Survey of Polar Wind From Mass-Resolved Tide Data

[10] In order to characterize the low-energy polar wind outflow, data from the TIDE instrument on board the Polar satellite have been analyzed. Up to about 5000 km altitude, the polar wind source function is found to be highly dynamic [e.g., *Abe et al.*, 1993; *Yau and Andre*, 1997]. However, above 5000 km much of the low-energy ion transport is easier to characterize with straightforward electric and magnetic field convection models. The Polar orbit perigee during 1996 took the spacecraft over the southern polar cap at altitudes of approximately 5000 km, giving the TIDE instrument the opportunity to collect a large data set of polar wind outflow measurements at this altitude, in the fall to winter season in the southern hemisphere. TIDE's ability to measure the full mass-resolved ion distribution function allowed us to obtain good estimates of mass-resolved fluxes, pitch angles, and energies of the upflowing ions over the entire southern polar cap.

[11] There are some notable limitations to this survey. Most regrettably, the Plasma Source Instrument, a companion instrument to TIDE designed to minimize the spacecraft floating potential, was only activated near orbital apogee during 1996. Thus spacecraft charging was still a factor in the low-altitude portion of the data set and had to be accounted for through data analysis methods. Also, during this time period, TIDE was operational only at L shells greater than 8, or about 68 degrees invariant latitude, to avoid instrument exposure to dangerous high-energy particles in the radiation belts. The 1996 time period fell during solar minimum so magnetic activity was generally low ($Kp \leq 4$) during the entire survey.

[12] Finally, only H^+ distributions were analyzed. Very low count rates of He^+ in the TIDE instrument [see *Su et al.*, 1998a] indicate that helium outflows have significantly lower fluxes than hydrogen and possibly that He^+ energies are low enough to allow spacecraft charging to prevent their detection by TIDE. Previous polar wind outflow studies [*Chandler et al.*, 1991; *Sojka et al.*, 1983; *Brinton et al.*, 1971] suggest that helium should be present at these altitudes with outflow characteristics similar to hydrogen but with fluxes of about a factor of 10 to 100 less than the H^+ fluxes. The helium to hydrogen outflow velocity ratio was also seen in these studies to increase with altitude from about 0.1 near 2000 km to 0.5 at 20,000 km. Other reports [*Lund et al.*, 1998; *Collin et al.*, 1988] suggest that helium fluxes can occasionally be much greater. However, at Polar perigee altitudes, He^+ energies are still small enough to result in observations being strongly affected by spacecraft potential. Typical flow velocities of 3 km s^{-1} translate to only 0.2 eV in energy. This combined with the fact that He^+ fluxes are one to two orders of magnitude less than H^+ fluxes keeps the TIDE instrument from detecting unambiguous flows of He^+ polar wind over most perigee passes. Our particle trajectory mapping suggests that these low-energy polar wind He^+ ions with less than 3 eV are unable to escape the inner magnetosphere and contribute to the ionospheric supply of magnetospheric plasma. Thus for the purpose of this study, we consider only the more energetic auroral and cleft ion fountain outflows as sources for He^+ in the outer magnetosphere.

[13] Although O^+ definitely does escape from the ionosphere and some have previously reported this upflowing O^+ as polar wind [e.g., *Abe et al.*, 1993], oxygen outflows were traditionally not considered to be part of the "classical" polar wind [*Banks and Holzer*, 1968]. Typically, net upward flows of O^+ over the polar cap are only seen above 5000 km with the cleft ion fountain as their likely source [*Yau and Andre*, 1997; *Su et al.*, 1998a]. Good reviews of O^+ outflow exist in the literature [e.g., *Yau et al.*, 1988; *Pollock et al.*, 1990; *Abe et al.*, 1996; *Peterson et al.*, 2001; *Cully et al.*, 2003a] and will be discussed below under the heading of cleft ion fountain outflows.

[14] Polar wind events were designated based on TIDE data integrated over ten 6-s spins of the spacecraft to process the information on a 1-min timescale which corresponds to a latitudinal width of about 2 degrees. Each data array was transformed to the plasma frame (Figure 1) and only ions with energies less than 3.5 eV were considered in order to isolate the polar wind from more energetic ion populations. The pitch angles of these ions were then measured and the associated directional fluxes were placed into 10-degree pitch angle bins. Once the data were collected into energy-angle bins, a decision was made whether to classify the interval as a "polar wind event." Only events with directional fluxes above 10^5 ions cm^{-2} sr^{-1} s^{-1} and with smooth pitch angle spectra were chosen in order to assure convergence in the filling routine. This prevented low instrument count rate intervals with distorted phase space distribution functions, due to spacecraft charging, from being considered.

[15] If the time interval was designated as a "polar wind" detection, an iterative filling code [see *Su et al.*, 1998a] was then used to fit the three-dimensional distribution to a bi-Maxwellian. One of the input parameters crucial to this filling routine is an accurate input of the spacecraft potential. Here we have used direct onboard measurement of spacecraft potential from the Polar/EFI instrument [*Harvey et al.*, 1995] with a 2 volt correction applied to account for the bias of the EFI probe with respect to the ambient plasma [*Scudder et al.*, 2000]. Once the iterative filling routine converged, revised moments were calculated for the selected interval. Flux values were adjusted to a common altitude of 5000 km, although the effects of the altitude range of this study were small. These data files were then assembled into one statistical database from which the following results were obtained. It should be noted that the 2 volt spacecraft potential correction has been determined using direct measurements of the photoelectrons and ambient electrons around the polar spacecraft from the Polar/HYDRA instrument [*Scudder et al.*, 1995]. Thus the critically important

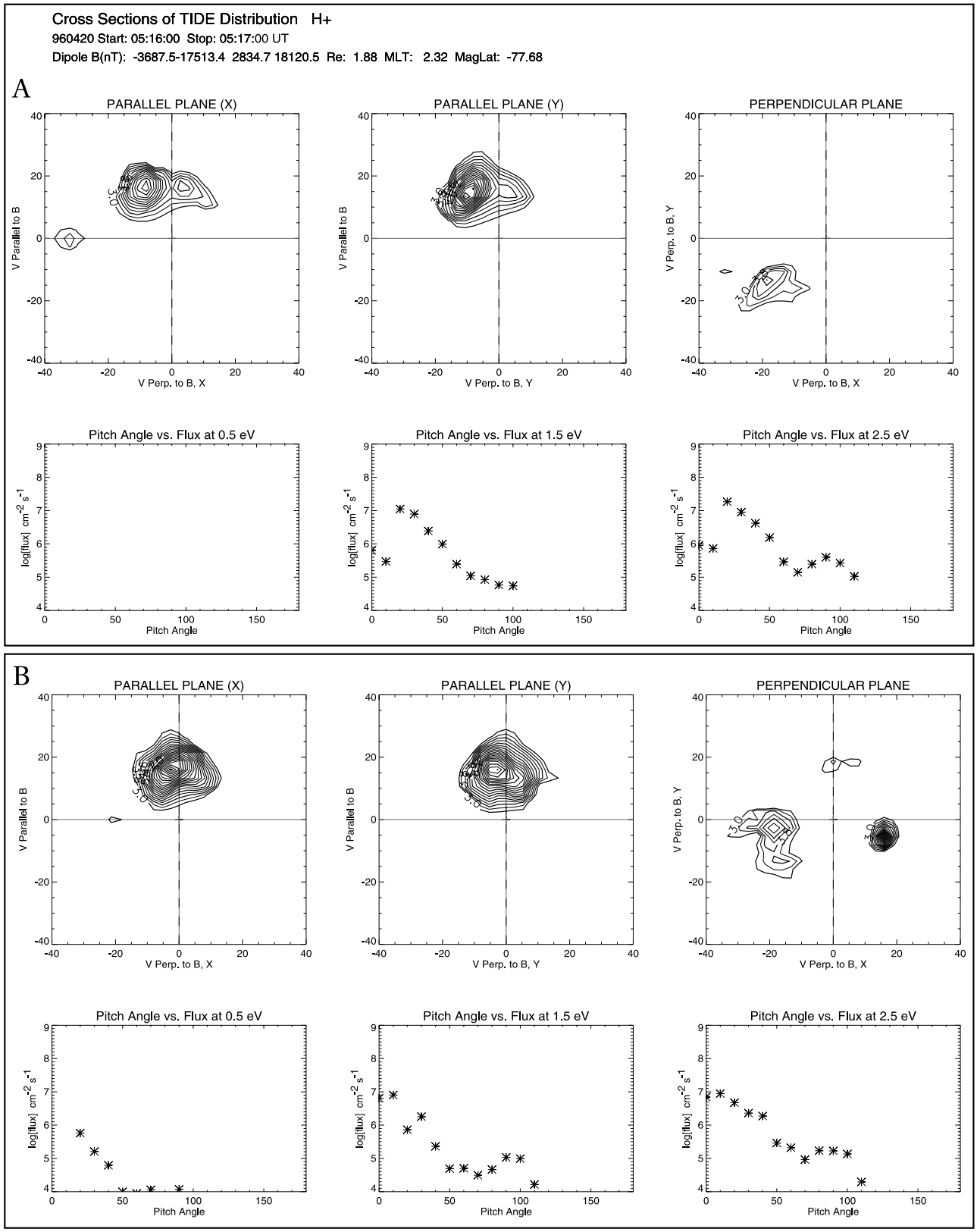

Figure 1. Polar wind H^+ distributions (a) before and (b) after correcting for plasma drift. The ion distributions are displayed in velocity space as contour plots in a magnetic coordinate system with one axis aligned with the local magnetic field direction, one axis in the direction of the cross product of the plasma bulk velocity and the magnetic field (labeled "X"), and the third axis (labeled "Y") completing the right-hand system.

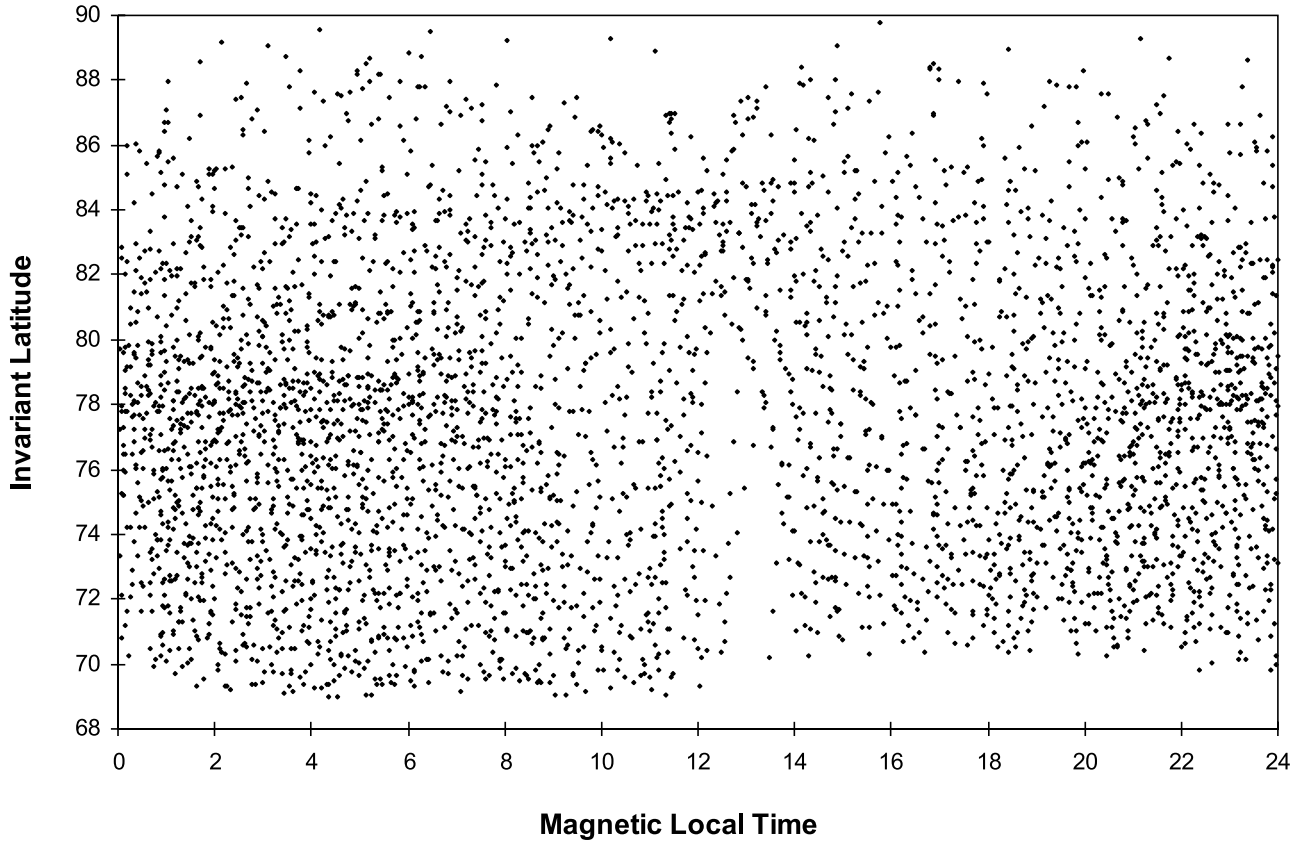

Figure 2. The total sample space of this survey.

parameter of spacecraft potential has been directly measured by two instruments on board Polar. This potential measurement is very significant in the calculation of the low-energy ion flux. Although the original *Su et al.* [1998a] analysis utilized the spacecraft potential measured by EFI that was available at that time, it did not include the more recent correction determined by the *Scudder et al.* [2000] analysis. When this 2 volt correction is included, it can increase the derived upward H^+ flux by as much as a factor of 5!

4. Data and Discussion

[16] Figure 2 shows the sample space in invariant latitude and magnetic local time of the TIDE data set from 29 March 1996 through 31 August 1996. The spacecraft altitude was generally within 1000 km of the average value of 5600 km. A small decrease in the density of samples is apparent between 13 and 16 hours magnetic local time. Otherwise the coverage is quite good for all latitudes above 69 degrees.

[17] The dramatic effect of spacecraft charging on polar wind observations is seen in Figure 3. The occurrence number of all 1-min samples in the data set (gray) and samples where polar wind is detected (black) are both plotted against spacecraft potential (as measured by Polar/EFI with a 2 volt correction). Although most of the time the spacecraft was charged to higher than 5 volts positive, the majority of polar wind detections occurred when the spacecraft potential was less than 5 volts. Figure 4 shows the probability of observing a polar wind "event" as a function of measured spacecraft potential. The likelihood of seeing

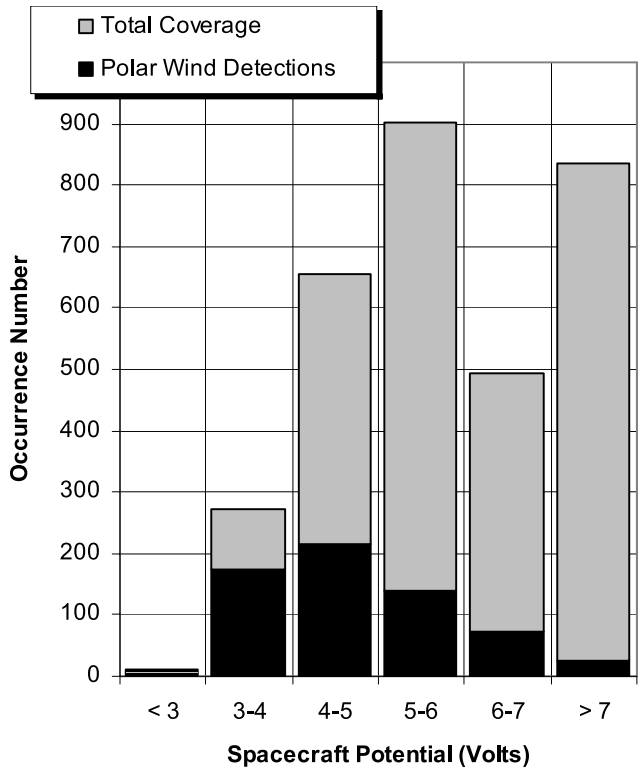

Figure 3. Polar wind detections and total sample space versus spacecraft potential.

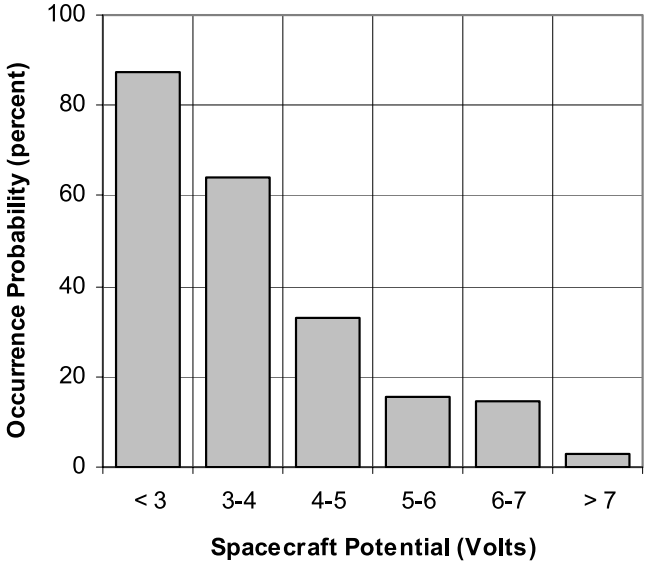

Figure 4. Polar wind occurrence probability versus spacecraft potential.

polar wind decreases monotonically with increased spacecraft charging. When the satellite was charged to less than 3 volts, the occurrence probability is near 90 percent.

[18] A relatively steady H^+ polar wind outflow, as theory [*Banks and Holzer*, 1968] and models [*Schunk*, 1988] predict, is completely consistent with these TIDE observations. We know that at higher altitudes, large ubiquitous H^+ outflows are completely masked by spacecraft potential. This is demonstrated by the sample TIDE spectrogram shown in Figure 5. In this spectrogram, taken near Polar apogee, very sparse and sporadic H^+ outflow is observed until 2145 UT when the Plasma Source Instrument (PSI) is activated. As long as the PSI is operational, the spacecraft potential is held to about 2 volts positive and a strong H^+ outflowing flux is continuously visible. In other orbits across the polar cap and magnetotail lobes, when the PSI is not operating, there is almost no observed H^+ outflow. The variable in this situation is not the H+ outflow but the spacecraft potential that is being controlled by the PSI plasma emission. Because of the dramatic nature of the appearing H^+ flux at this high altitude, the acceptance of the influence of spacecraft potential for this region has been more straightforward. *Su et al.* [1998a] reports that when PSI is activated, H^+ outflows at these altitudes are not sporadic events but rather long duration outflows lasting several hours over the course of the Polar apogee across the polar cap.

[19] The continuous polar wind fluxes observed at high altitudes are connected to the steady polar wind source at 5000 km. This steady outflow cannot completely be directly observed, however, since the masking effects of a positive spacecraft potential are also important at lower altitudes during Polar perigee passes. It is our interpretation that the polar wind is, in fact, always present but usually hidden from view by the spacecraft potential. This is consistent with the decision to disregard low flux events. Since the measured flux events (directional fluxes above 10^5 cm^{-2} sr^{-1} s^{-1}) appear to be omnipresent when ion measurements are not obstructed by high spacecraft potentials, considering only these fluxes should not unfairly bias the data toward higher values than the true unobstructed polar wind flux.

[20] Table 1 illustrates some of the interesting consequences resulting from the use of corrected values of spacecraft potential as well as a larger data set. The revised fluxes of 6.0×10^7 ions cm^{-2} s^{-1} are consistent with theoretical expectations [e.g., *Schunk and Sojka*, 1997] and about 5 times higher than the published values of *Su et al.* [1998a]. The parallel velocities are slightly higher, but the most significant change is seen in the polar wind densities which are about 3 times greater. There also appears to be less of a difference between perpendicular and parallel ion temperatures than was previously reported, though perpendicular temperatures are seen to be about 1.5 times larger than parallel temperatures on average.

[21] Derived fluxes from this survey are plotted versus day of year in Figure 6, showing that the data analyzed were taken during local winter conditions. Although the spread in the data is large, the maximum fluxes appear to decrease significantly very near winter solstice. This is consistent with previous DE measurements which reported maximum polar wind outflow occurring during local spring [*Chandler et al.*, 1991]. Because this survey covered high latitudes during local winter, solar zenith angles were generally large as seen in Figure 7. Over 91 percent of the polar wind events studied were associated with zenith angles greater than 90 degrees, indicating that the ionosphere from which the polar wind originated was receiving less direct sunlight. One would thus expect that these fluxes are less than that of the polar wind emerging from the dayside ionosphere [*Sojka and Schunk*, 1983]. Nearly all of the data were acquired during magnetically quiet times ($Kp \leq 4$), and no clear significant variation was seen as a function of *Kp*.

5. Polar Wind Input Grid

[22] Figure 8 summarizes the results from this survey that provide numerical bounds for polar wind H^+ energies and pitch angles as a function of location for invariant latitudes greater than 70 degrees. These bounds are based on the typical range of ion pitch angles found in each location bin determined from the pitch angle spectra such as those shown in Figure 1. Both the energy and pitch angle ranges shown in Figure 8 were chosen as FWHM (full-width half maximum of the distribution function) bounding values to represent the bulk of the ion distribution.

[23] It is clear from Figure 8 that more field aligned distributions with higher flow velocities originate in the morning sector. Between 70 and 75 degrees invariant latitude, the polar wind velocity spread is largest near dawn, possibly indicating higher ion temperatures in this region. Polar wind fluxes, when corrected for spacecraft charging, did not vary with statistical significance with location. Thus the value of 6.0×10^7 ions cm^{-2} s^{-1} from Table 1 appears to be a good estimate to use for true polar wind H^+ fluxes at 5000 km altitudes and above 70 degrees invariant latitude for magnetically quiet, high zenith angle conditions.

[24] For lower latitudes between 60° and 70°, the energy range of 0–3 eV and pitch angles from 0 to 60 degrees were used for modeling. This estimate should provide reasonable upper and lower bounds for H^+ polar wind distributions in

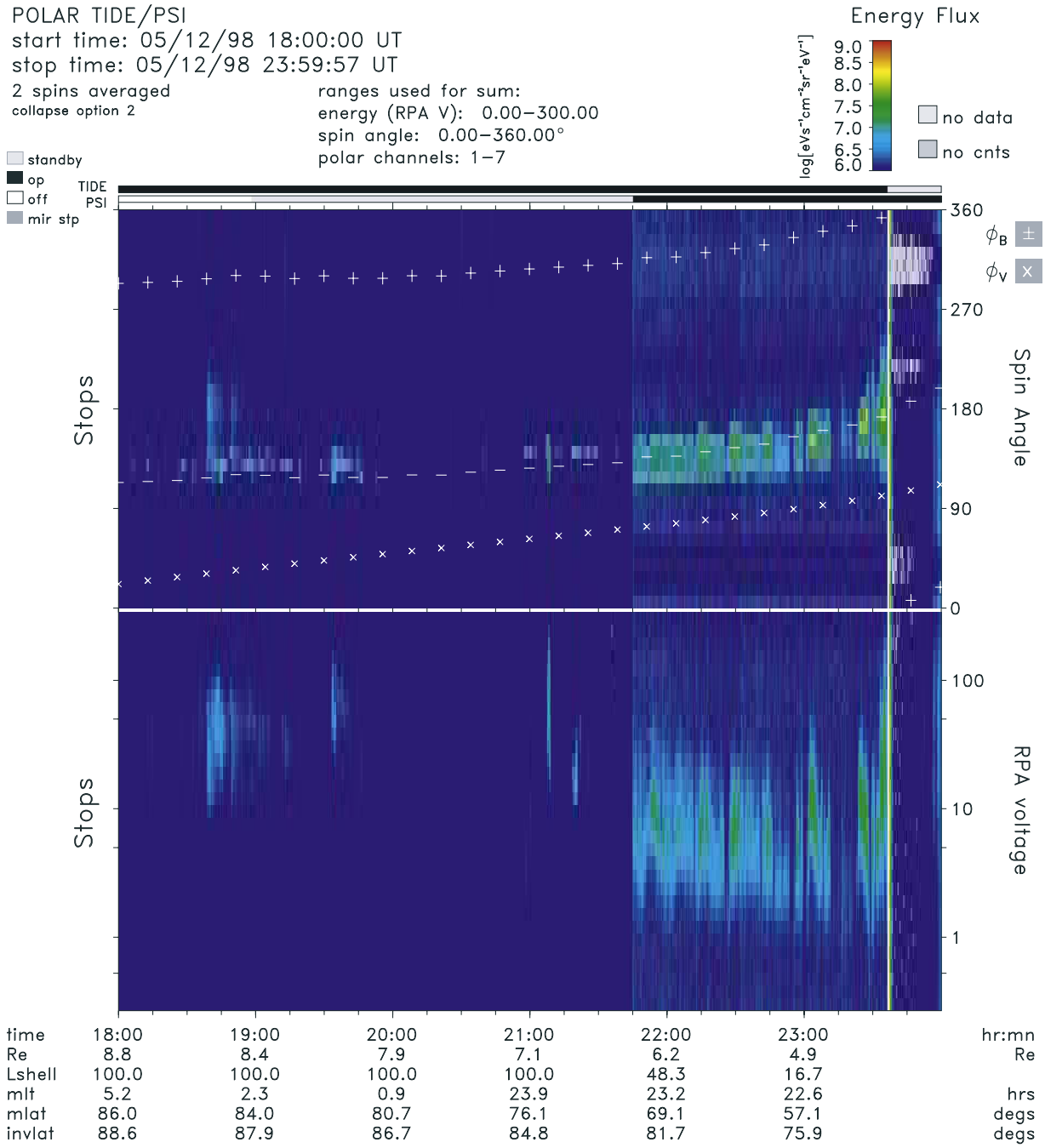

Figure 5. A TIDE pass across the polar cap and magnetotail lobe with the PSI turning on during the pass at 2145 UT. Outflows of less than 10 eV are hidden from view until PSI is activated.

Table 1. Characteristics of Polar Wind H^+ Outflows[a]

Polar Wind	Average Flux, $\times 10^7$ ions cm^{-2} s^{-1}	$V_{\|\|}$, km/s	Density, ions cm^{-3}	$Temp_{\|\|}/Temp_{\perp}$, eV
Results from uncorrected EFI [*Su et al.*, 1998a]	1.2	15	~10	0.46
Results when correcting for EFI probe bias	6.0	17	34	0.67

[a]In the first row are moments calculated by *Su et al.* [1998a], without correcting for the EFI probe bias (from TIDE measurements during April 1996) The second row shows moments resulting from the iterative filling routine of *Su et al.* [1998a] using spacecraft potentials corrected for EFI probe bias with respect to the ambient plasma (from TIDE measurements covering 29 March 1996 through 31 August 1996). Fluxes are adjusted to 5000 km altitude.

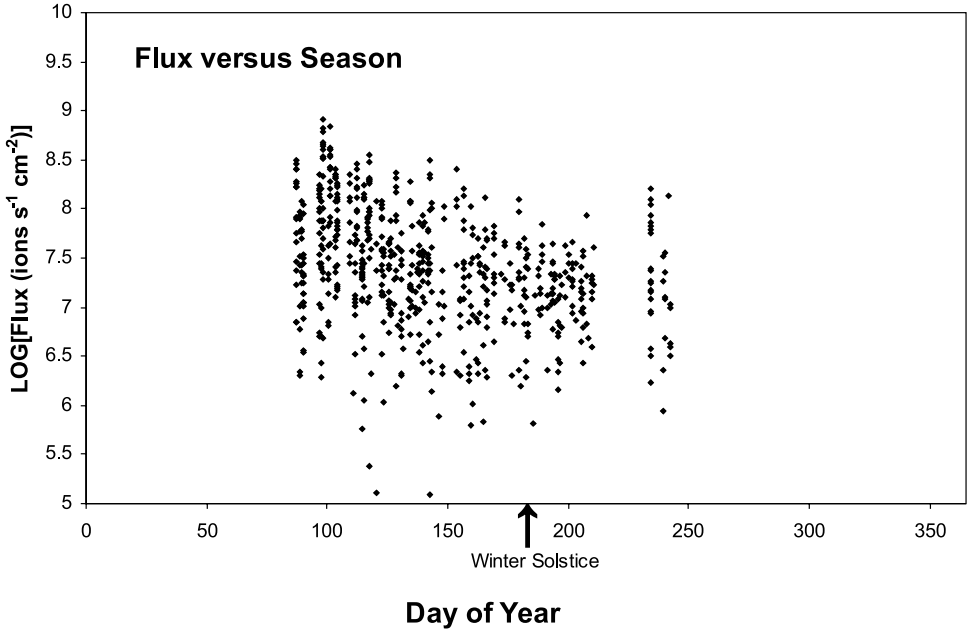

Figure 6. Corrected polar wind H^+ flux versus day-of-year for our survey using TIDE data from 29 March 1996 through 31 August 1996.

this region as well because the polar wind is generally expected to flow with full strength into flux tubes outside of the average plasmapause position at 60° invariant latitude since these flux tubes reach diffusive equilibrium only in periods of extended quiet. H^+ fluxes of 6×10^7 ions cm^{-2} s^{-1} were used in this study although previous studies have suggested H^+ outflow could be even greater at lower latitudes [e.g., *Abe et al.*, 1996]. Polar wind originating from sub-auroral latitudes is an important source region for the plasma sheet, as shown in the ion trajectory modeling below, and needs to be taken into consideration when modeling the total outflow [see *Elphic et al.*, 1997].

6. Model Trajectory Results

[25] Ion trajectories were calculated using a modified version of the steady-state three-dimensional particle tracing FORTRAN code described by *Sauvaud and Delcourt* [1987]. It includes numerical procedures developed by *Delcourt* [1985] and subsequent modifications by *Delcourt*

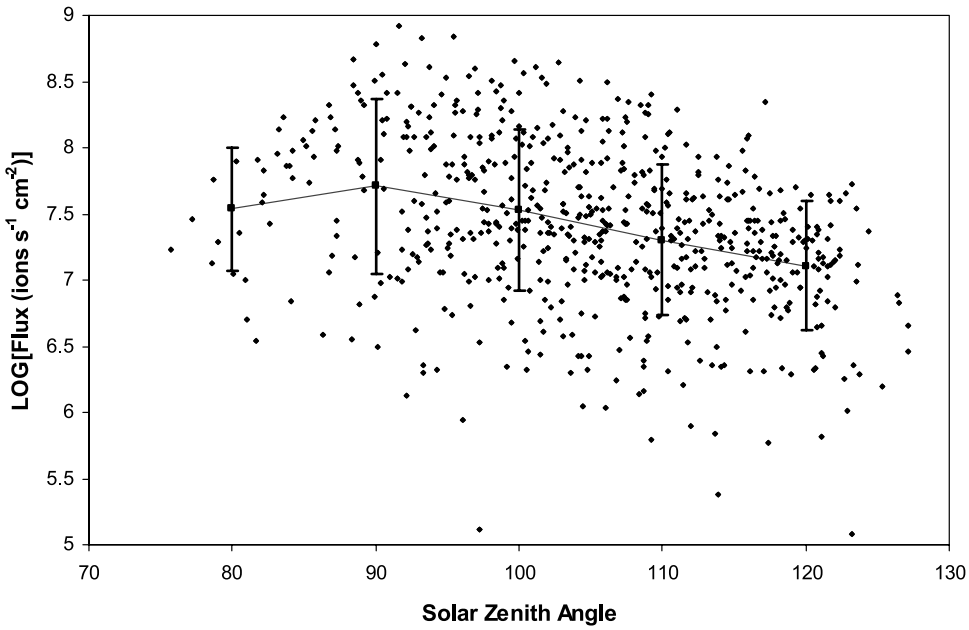

Figure 7. Corrected polar wind H^+ flux versus solar zenith angle. Binned averages showing errors of 1 standard deviation are plotted on top of the data.

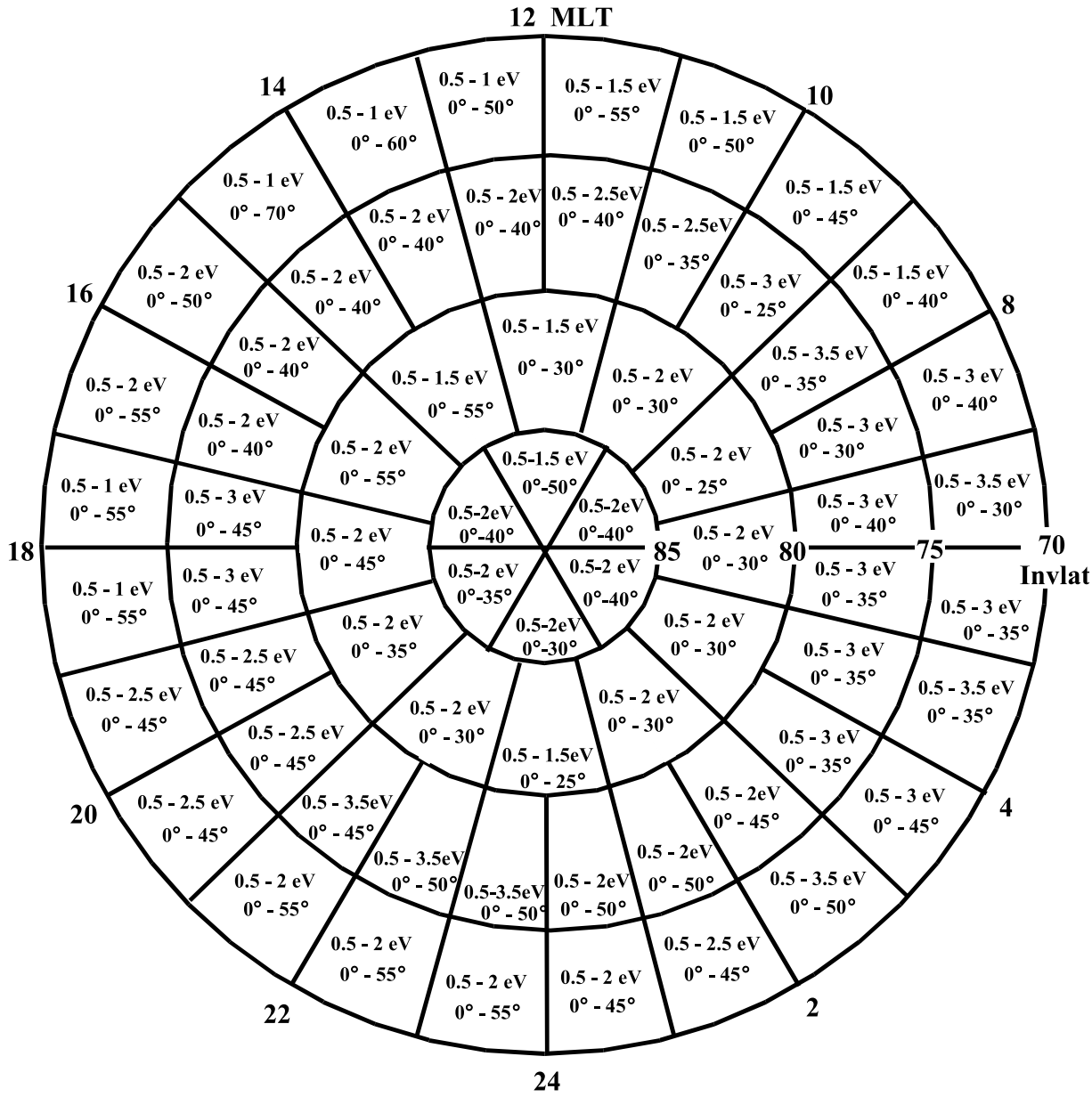

Figure 8. Polar wind input grid: energy and pitch angle range versus location for a source altitude of 5000 km.

et al. [1988, 1989, 1993]. At low altitudes, it uses guiding center approximations to track ions. Full Lorenz-force particle trajectory calculations are used once ions exceed 2 R_E geocentric. The trajectory code traces one ion at a time until the particle reaches the preset spatial boundaries of the magnetosphere in the code or until a specified lifetime of the particle has elapsed.

[26] Calculations take into account the dipole tilt of the Earth's magnetic field using the semiempirical Tsyganenko '89 magnetic field model [*Tsyganenko*, 1989]. This model contains six sets of driving parameters, making it dependant on a given value of *Kp*. The trajectory code maps electric field potentials to the ionosphere using a Volland electric field model with a Heelis correction [*Volland*, 1979]. The Volland model is semianalytic and dependent on quasi-static electric potential fields.

[27] The code takes initial values of energy, mass, pitch angle, local time, and magnetic latitude as inputs and recalculates each parameter except mass iteratively until the boundaries of the model are encountered. The code is not able to model the magnetosheath region or any regions outside of the model magnetosphere. If an ion travels into the magnetosheath or beyond a distance of 70 R_E, the code calculations are automatically terminated. Also, a low-altitude boundary of 0.1 R_E (approximately 600 km) was set for the trajectories run in this study. Collisions begin to become important in the ionosphere at altitudes below 2000 km [*Barakat et al.*, 1995], and ions that penetrate to 600 km have little chance of mirroring before being scattered. This scattering may not necessarily imply that these ions are immediately lost to the ionosphere. However, our software cannot model ionospheric collisions at this

time; thus we will assume for the purposes of this study that ions reaching a depth of 600 km remain in the ionosphere and do not mirror back out.

[28] The particle trajectory code was used to model all possible types of ionospheric outflow. The most extensive set of trajectory calculations was performed for polar wind ions. For these ions observed statistical polar wind characteristics from the TIDE instrument were used as a set of specific input parameters to the trajectory model (see Figure 8). Both H^+ and He^+ polar wind ions were modeled. Two sets of ion trajectories were calculated with the code configured for quiet and moderate levels of magnetic activity.

[29] Trajectories were also run for H^+, He^+, and O^+ cleft ion fountain ions exiting the ionosphere. These ions were initiated with energies and pitch angles selected to represent typical cleft ion fountain characteristics [*Pollock et al.*, 1990; *Cully et al.*, 2003a]. Finally, auroral ion outflows were modeled by starting H^+ and O^+ ions at energies of 500 eV or more from within typical auroral latitudes.

[30] Particle trajectories were run for H^+ ions using the bounding input parameters shown in Figure 8. They were grouped into four basic input bounding limits: minimum energy–minimum pitch angle, minimum energy–maximum pitch angle, maximum energy–minimum pitch angle, and maximum energy–maximum pitch angle. For each energy/pitch angle combination, the code was used to track 114 different trajectories representing all local times and invariant latitudes greater than 60 degrees. For latitudes between 60 and 70 degrees, TIDE polar wind statistics were lacking. In these locations we used upper and lower bounding estimates of 0–3 eV energies and 0–60 degrees pitch angles, obtained by extrapolating from the higher-latitude regions. Below 60 degrees, upflowing ions tend to be captured in the plasmasphere and hence are not available as a direct source for magnetospheric plasma. All ions were initiated at 5000 km altitude to correspond with the approximate altitude of TIDE polar wind measurements. The resulting trajectories, calculated for each of the four sets of input parameters, demonstrate the variety of paths taken by ions within the bulk polar wind distribution exiting a particular location above the ionosphere. By running these trajectories, a great variety of possible ''fates'' for polar wind ions was discovered. A classification system was developed based on energies and magnetospheric regions that a particular ion traverses. This system helped us keep track of the different basic behaviors that ion trajectories typically displayed. A single ion trajectory would often require a series of classifications as the ion passed from region to region within the magnetosphere.

6.1. Precipitating and Escaping Ions

[31] One possible fate for a polar wind H^+ ion is for it to simply precipitate in the conjugate ionosphere. The trajectory calculations are halted when an ion descends to 600 km since it is assumed that below this altitude, ions will be unable to mirror but instead be collisionally scattered into the ionosphere. In general, ions originating at low latitudes with zero pitch angles were likely to exhibit this behavior. Energies over the entire ion path would usually stay below 10 eV. If however, the ion passed through the near-tail region, it could pick up more than 100 eV before precipitating in the conjugate ionosphere.

[32] Another possible end to a trajectory is for the ion to exit the bounds of the model magnetosphere at which point the particle is assumed to enter the magnetosheath. These ions drifts to larger L shells as they travel upward until they finally reach the magnetosphere boundary. Although the trajectory code is halted when an ion enters the magnetosheath, it does not necessarily imply that an ion is ''lost'' from the magnetosphere. It is very likely that some magnetosheath ions are capable of reentering the magnetosphere, particularly along the flanks of the magnetotail. However, the limits of the present model prevent an accurate description and quantification of these ions.

6.2. Convection Dominated "Bouncing" Ions

[33] A polar wind ion with a larger initial pitch angle would often reflect between hemispheres. The energies of these ''bouncing'' ions [see *Delcourt et al.*, 1988] could vary from a few eV to greater than one keV but were typically low enough in energy to result in motion dominated by magnetospheric convection rather than simple curvature drift. Bouncing ions could eventually attain a variety of pitch angles. Some remained fairly field aligned and reflected at low altitudes within the ionosphere. However, if the ion received extra perpendicular energy from convection electric fields, its pitch angle could increase to the point where it became trapped near equatorial magnetic latitudes.

[34] Ion trajectories that we classified as ''bouncing'' were always convection dominated. These ions would travel in the direction of the Earth's rotation up until around noon magnetic local time, which would typically take several hours flight time. Often ions would convect past noon through the afternoon sector, though it was rare for a trajectory to travel past 15 hours magnetic local time. At some point, however, the reflecting ion would either be swept into the magnetosheath, precipitate in the ionosphere, or bounce out to some other magnetospheric location (e.g., the plasma sheet).

[35] Figure 9 depicts an ion that begins by bouncing between hemispheres with less than 10 eV and losing energy as it convects sunward. Just past noon, the ion skims the northern pole and heads down tail far enough to pick up additional energy by curvature drifting through the cross-tail electric field. The ion then begins bouncing sunward once more but now at a couple of hundred eV.

[36] In the early evening sector where the sunward convection field and the corotation field are competing, bouncing ions often became trapped in local time. Figure 10 is an example of this case. The ion shows a complicated variation in energy as it drifts through higher L shells. The ion gains energy as it flows from north to south and loses energy as it flows back from south to north. This variation is most likely due to the fact that the ion is reflecting at slightly different latitudes and local times as it bounces in the northern and southern hemispheres. The pitch angle steadily increases so the particle mirrors at increasing altitudes. Instead of decisively drifting east or west, the ion instead drifts up and out into the magnetosheath.

[37] Trajectories similar to Figure 10 are common for ions originating in the evening sector at invariant latitudes

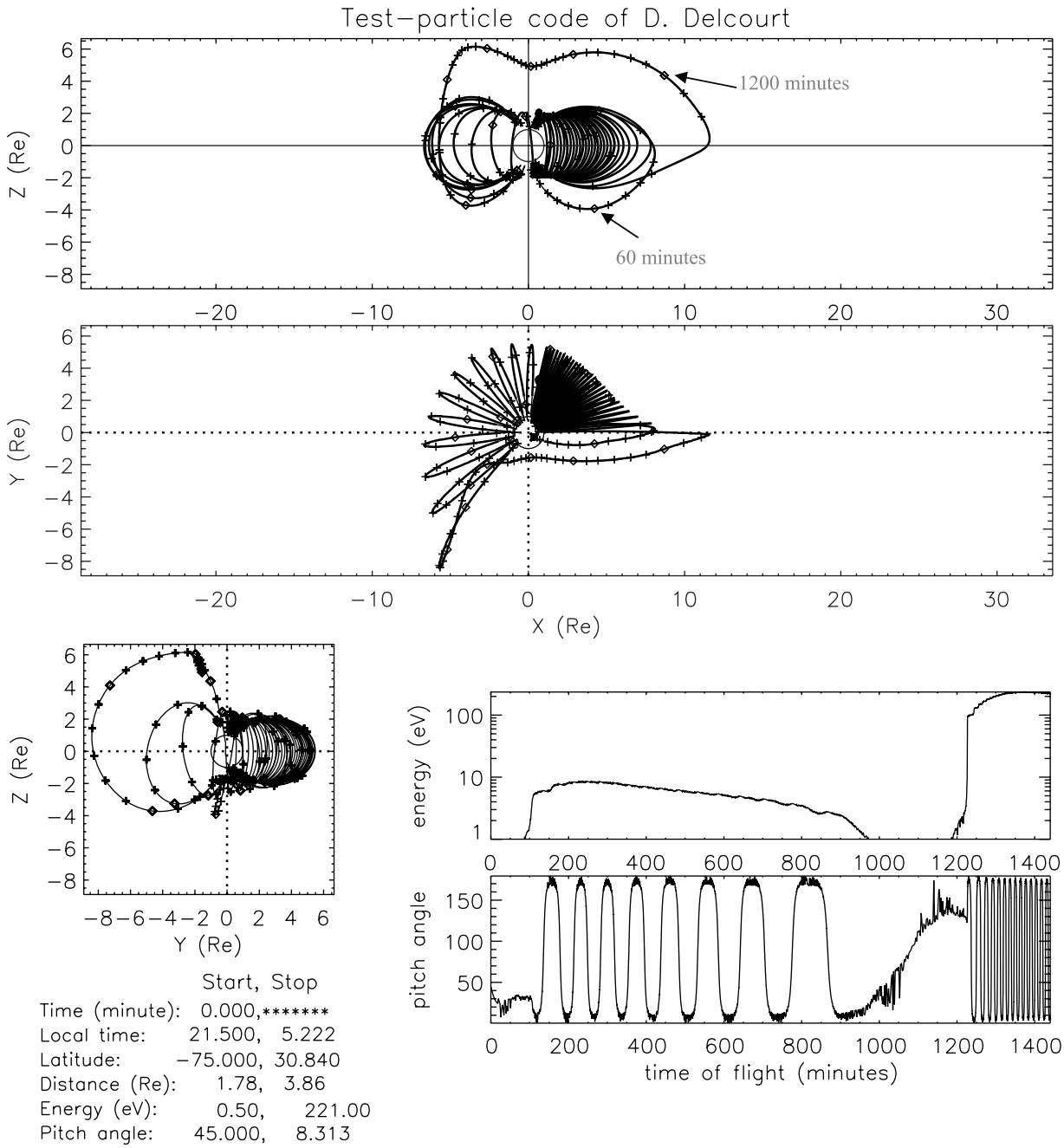

Figure 9. Sample trajectory of a polar wind ion that cycles through the dawnside twice as a convecting, "bouncing" ion at two very different energies. The Z-axis is aligned with the Earth's magnetic north pole, the X-axis points away from the Sun, and the Y-axis points toward dawn completing a right-hand system. Plus marks along the ion trajectory indicate 10-min intervals, while diamonds indicate hour-long intervals. A few sample times are labeled for reference in the top panel. The start and stop parameters are given in the lower left hand corner of the plot. The ion begins at 21.5 hours local time, −75 degrees magnetic latitude, and 1.78 R_E geocentric distance, with 0.5 eV energy and a pitch angle of 45 degrees from the field aligned direction.

between 65 and 75 degrees. These ions rarely exceed a few hundred eV before they enter the magnetosheath. It is important to note that these bouncing ions would appear very similar to counterstreaming precipitating ions as observed by an orbiting ion instrument, especially at equatorial latitudes where both distributions would be nearly field aligned. This may also contribute to the "bulge region" of the plasmasphere which is found at this range of local times [*Carpenter*, 1963].

6.3. Plasma Sheet and Ring Current Ions

[38] Often polar wind ions will journey out through the magnetotail where an interesting series of acceleration mechanisms can greatly increase ion energy to values

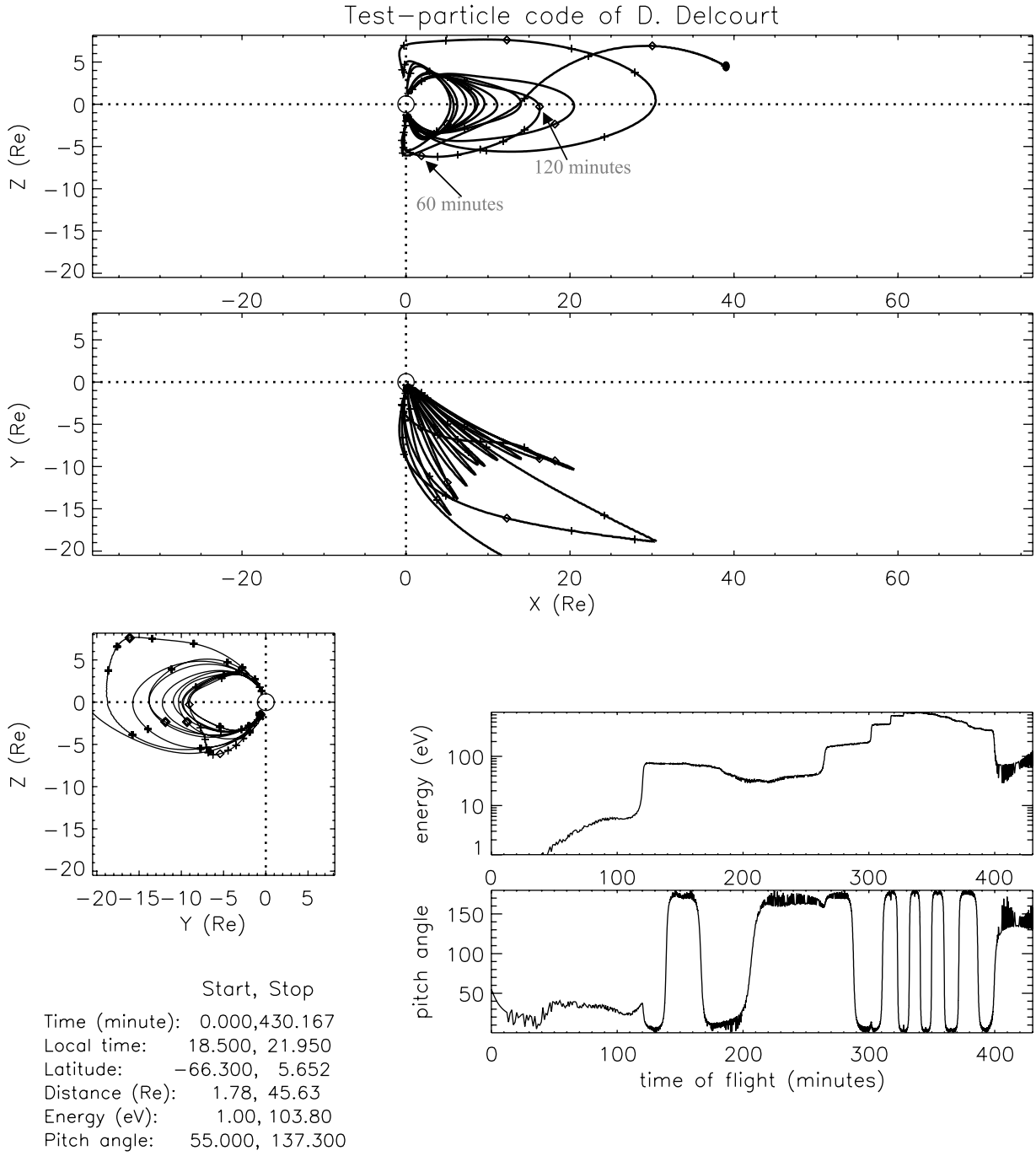

Figure 10. Sample trajectory of a polar wind ion that remains nearly stationary in local time due to competing convection and corotating drifts. Start and stop parameters for the ion are given in the lower left-hand corner of the plot.

exceeding 0.5 keV. Figure 11 shows a segment of a typical trajectory where a polar wind particle becomes part of the plasma sheet. Initially, the ion loses kinetic energy as it fights the Earth's gravity. However, as it experiences magnetic curvature drift through the convection electric field potential, the particle gains energy that sends it across the polar cap into the lobes of the magnetosphere. This represents the so-called "centrifugal acceleration" mechanism described by *Cladis* [1986], *Delcourt et al.* [1993], and *Horwitz et al.* [1994].

[39] The basic analogy behind the name for this energization mechanism is that just as beads on a rotating wire are flung outward, ions accelerate upward as magnetic field lines sweep antisunward across the poles. Magnetic mirror forces decrease the pitch angle of the ion as it travels out to regions of lower magnetic field strength in the distant tail. At the neutral sheet, the ion travels through a highly curved magnetic field. It then curvature-drifts through the large cross-tail potential. This rapidly accelerates the ion which remains confined within the plasma sheet due to "centrif-

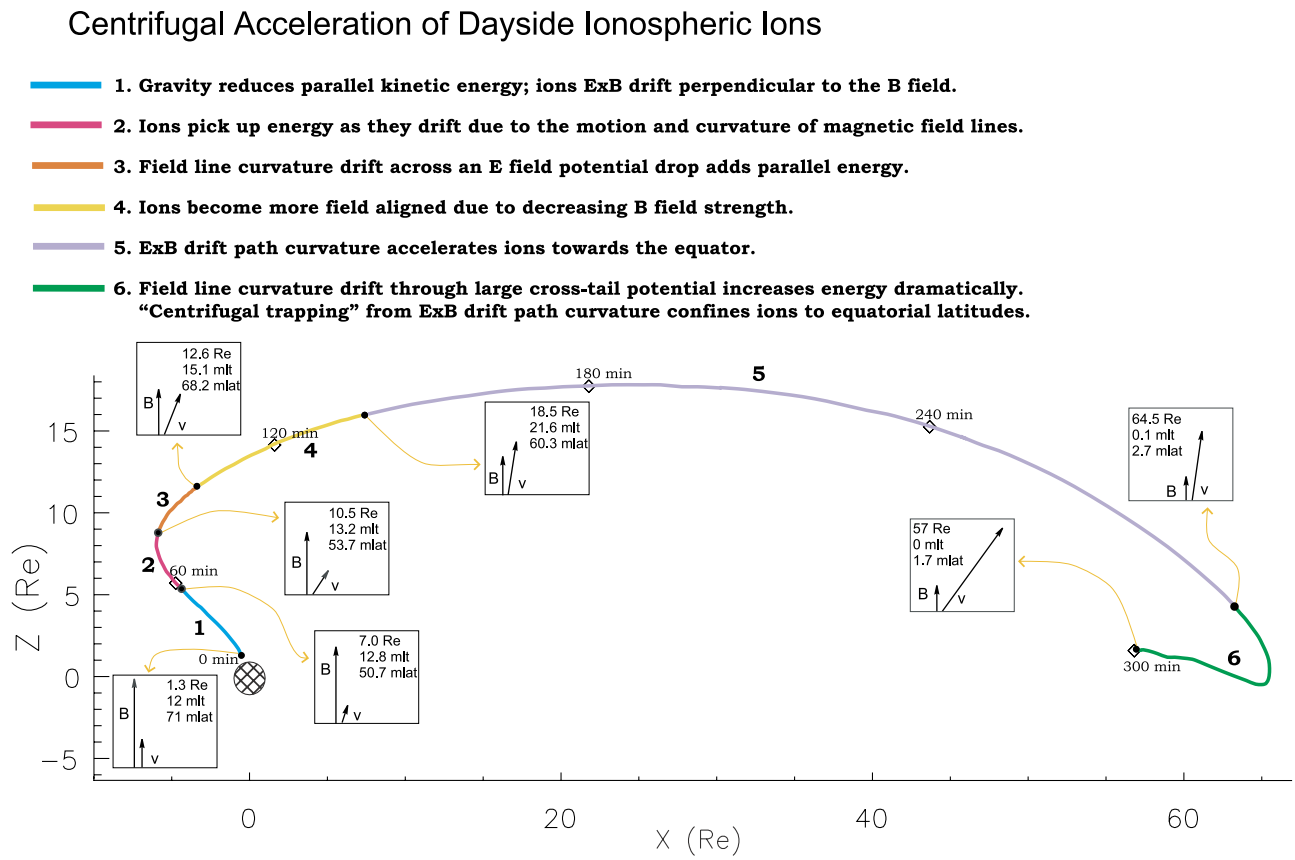

Figure 11. Typical acceleration of polar wind ions to form the plasma sheet. Six segments of the ion flight path are highlighted in different colors. Above the figure are basic explanations of the changes that occur in the ion flight path during each segment. Seven boxes list altitude, magnetic local time, and magnetic latitude for the beginning and the end time of each segment. Arrows show relative changes in magnetic field strength and ion velocity, as well as pitch angle variations.

ugal trapping" [*Delcourt et al.*, 1995]. The ion travels earthward, either forming the ring current or becoming a lower-energy drifting and reflecting ion as described above. Figures 12 and 13 are examples of each possibility.

[40] In Figure 12 the ion energy rises abruptly from about 1 eV to 5 eV at 50 min into the ion flight time. This corresponds to centrifugal acceleration, occurring where magnetic field lines curve sharply toward the tail. The ion coasts along through the tail lobes with less than 10 eV until it reaches the plasma sheet about 45 R_E away from the Earth. At the plasma sheet, the energy rapidly increases to several hundred eV as the ion rushes earthward. By the time this ion (now a part of the plasma sheet) reaches the inner magnetosphere, it still has less than 1 keV. It then begins drifting eastward, losing energy, until it reaches the afternoon sector.

[41] The ion in Figure 13 starts with a very similar path. It receives a centrifugal boost of several eV approximately 100 min into its flight. This ion travels more than 55 R_E downtail before encountering the plasma sheet and turning earthward. When it reaches the inner magnetosphere, the ion has over 10 keV and promptly becomes part of the ring current. Looking at all of the trajectories for polar wind ions that entered the plasma sheet, it appears that those ions that came back to the inner magnetosphere with less than 3 keV tended to drift eastward while those with greater energies would drift westward and contribute to the ring current.

6.4. Circulating Ions

[42] One of the most interesting results of our ion trajectory modeling was that polar wind ions would frequently circulate through a number of the locations and energies described above in a relatively short period of time. Figure 14 provides one example of this process. We begin with a polar wind ion of less than 1 eV that is quickly accelerated to 10 eV. The ion "bounces" eastward until the early afternoon magnetic local time. Then it skims over the north pole and becomes a plasma sheet particle of almost 10 keV. The ion is energetic enough so that when it reaches the inner magnetosphere it becomes part of the ring current. All of this takes place in the space of 24 hours.

[43] Trajectories similar to Figure 14 underscore the idea that magnetospheric ions do not remain "fixed" or confined to one region of geospace. There was always a time limit (usually less than 24 hours) used in the code after which the program would automatically terminate calculations for the ion path. Often ions would still be within the magnetosphere when this time elapsed, and thus their ultimate fate is not calculated. It seems plausible that a polar wind ion under the proper initial conditions could circulate through the mag-

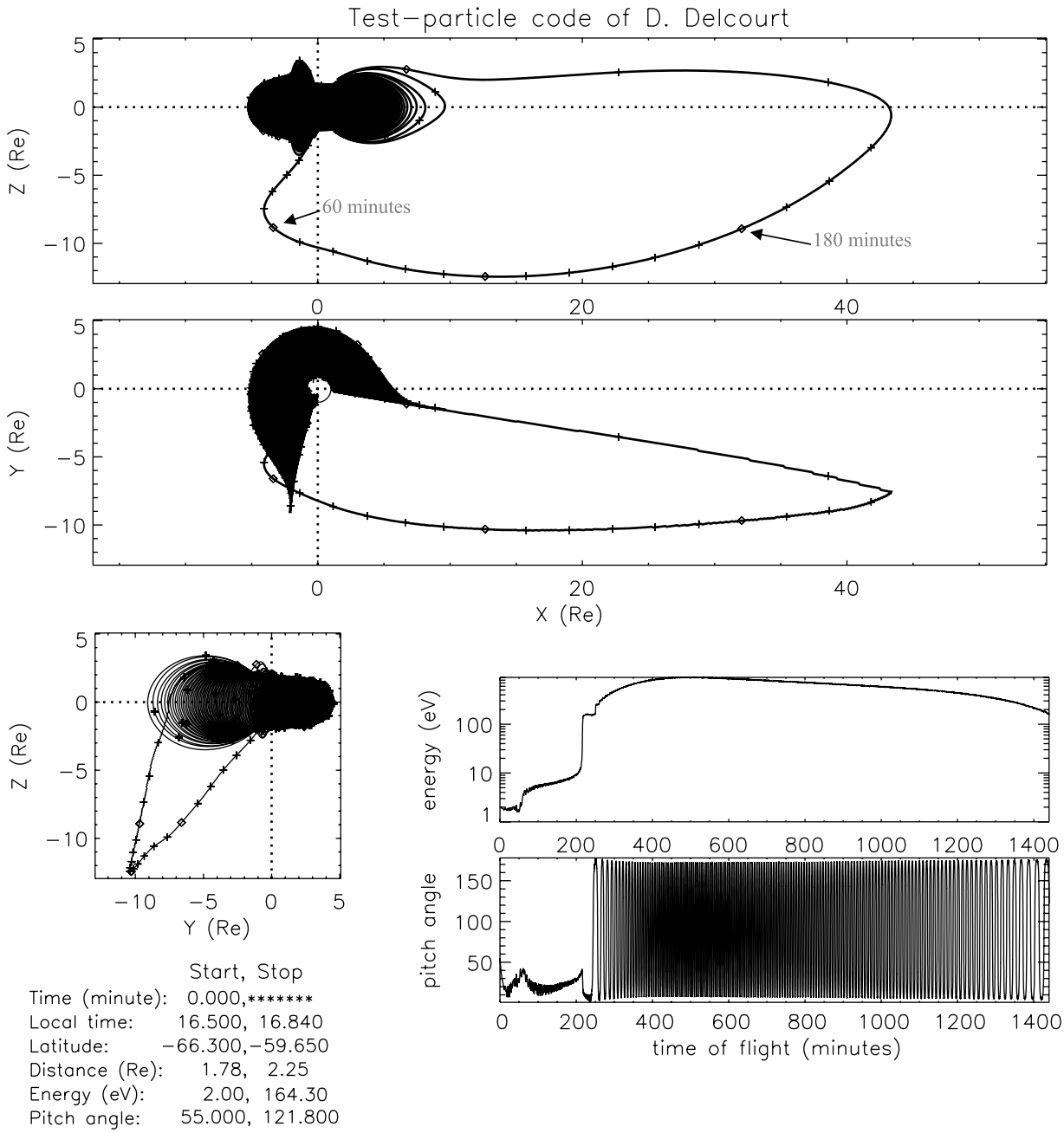

Figure 12. A sample trajectory of a polar wind ion that becomes part of the plasma sheet and then a bouncing convecting ion. Start and stop parameters for the ion are given in the lower left hand corner of the plot.

netosphere for at least several days, constantly changing its "identity" as it moves from region to region. This also implies that an ion only inhabits a specific region of geospace for a certain "residence time" before it is accelerated or decelerated through any number of possible mechanisms and drifts to become part of another plasma population in the magnetosphere.

7. Maps of Source Locations

[44] Figure 15 sums up all of the model trajectory results for polar wind H^+ exiting the southern hemisphere. Each of the four figures shows the characteristics of ion trajectories run at four different sets of initial conditions: minimum pitch angle–minimum energy (Figure 15a), maximum pitch angle–minimum energy (Figure 15b), minimum pitch angle–maximum energy (Figure 15c), and maximum pitch angle–maximum energy (Figure 15d). Color is used to indicate the energy range of the ion, while the letter represents location or behavior within the magnetosphere. One set of four inputs was run for each sector shown in the figures. A series of letters in a box indicates that the ion circulated through several energy ranges and/or locations during the modeled flight.

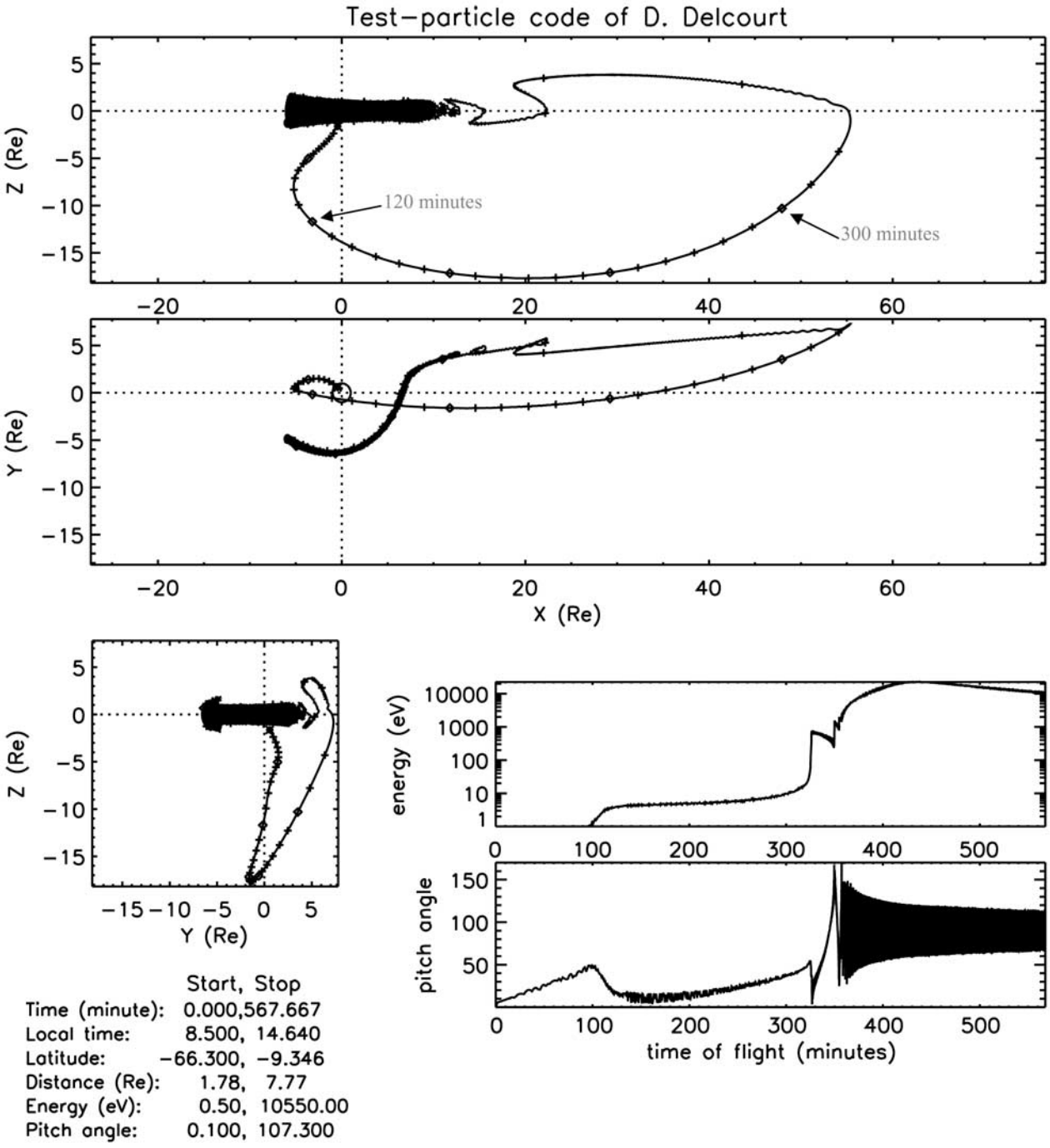

Figure 13. A sample trajectory of a polar wind ion that becomes part of the plasma sheet and then joins the ring current. Start and stop parameters for the ion are given in the lower left-hand corner of the plot.

[45] Numerous distinct patterns can be detected from these figures. In Figure 15a, one can see that polar wind ions heading straight up the field line at low energy (0.5 eV) tend to precipitate in the conjugate ionosphere when initiated at invariant latitudes lower than 65 degrees. This is consistent with the behavior of warm outer plasmaspheric ions. Ions heading out in the early morning hours often escaped into the magnetosheath. This was also true of ions from the early afternoon between 65 and 70 degrees invariant latitude. These ions could end up being lost to the interplanetary medium or could conceivably remain in the plasma mantle and be reintroduced to the magnetosphere in the distant tail lobes. Ions initiated from the dayside, especially between 70 and 85 degrees invariant latitude in the early afternoon, tended to form the plasma sheet and ring current. Farther away from noon, ions would still form the plasma sheet but would then enter the inner magnetosphere with less energy and become convection

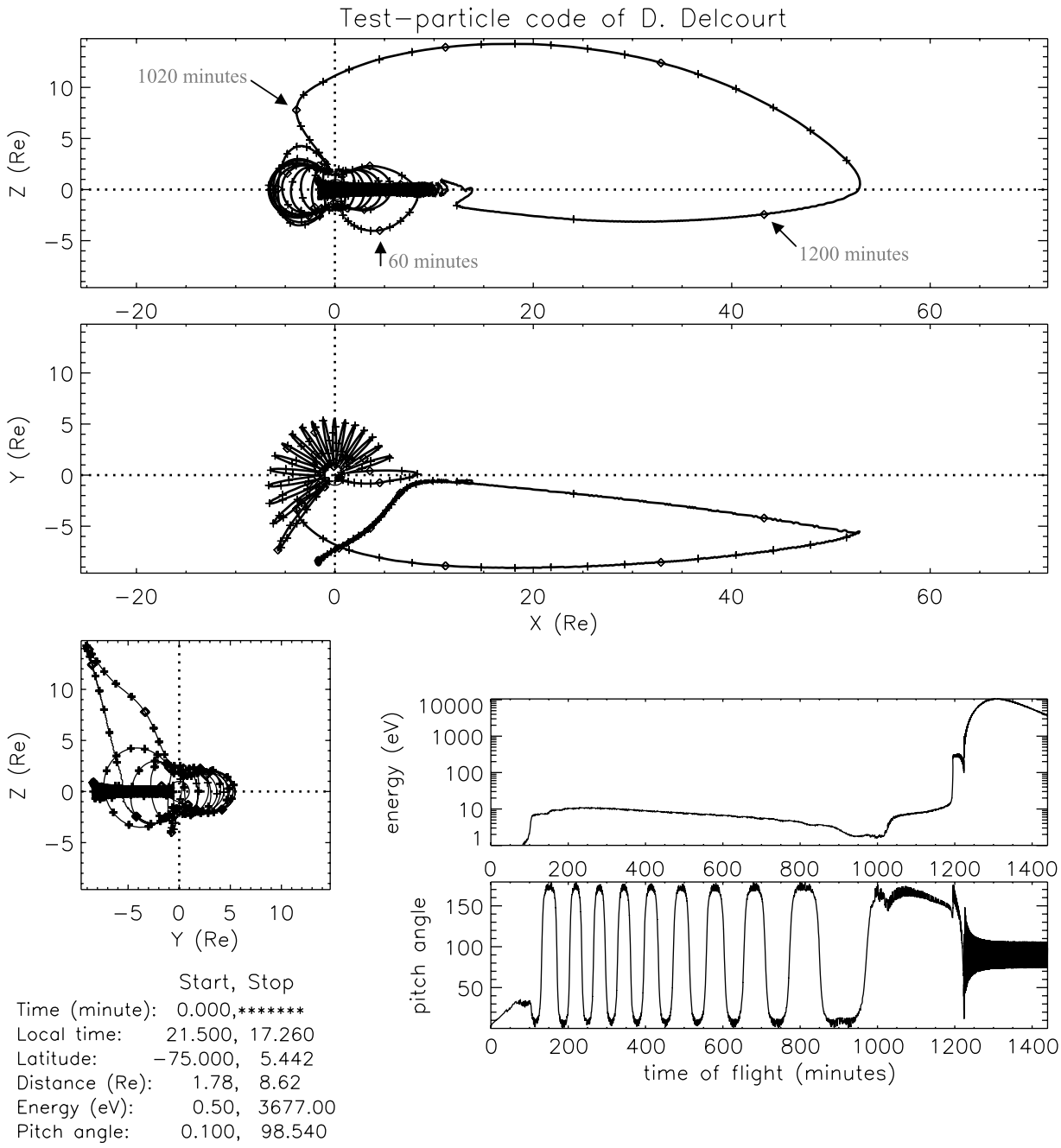

Figure 14. A sample trajectory that demonstrates ion circulation within the magnetosphere. Start and stop parameters for the ion are given in the lower left-hand corner of the plot.

dominated bouncing ions. In general, warm bouncing ions started near the pole and in the early evening hours, while cold bouncing trajectories were often seen originating in the early morning hours.

[46] In Figure 15b, ions have a higher initial pitch angle, changing the precipitating ions of Figure 15a to bouncing ions. However, particles that left the ionosphere at greater invariant latitudes could still precipitate. Both bouncing and precipitating ions in this region would still be consistent with characteristics of the outer plasmasphere. Other patterns seen in Figure 15a are very similar to those in Figure 15b, indicating that low-energy polar wind ions with differing initial pitch angles meet generally similar fates.

[47] In Figure 15c, trajectory characteristics are shown for polar wind ions with higher energies that initially flow straight up the field line. As in Figure 15a, this figure shows particles that start at low invariant latitudes tend to immediately precipitate. However there is a new band of midlatitude ions stretching from dawn to 1400 MLT that escape to the magnetosheath. There is also a noticeable group of polar wind ions that start in the high-latitude morning sector and precipitate in the conjugate ionosphere with slightly higher energies. Plasma

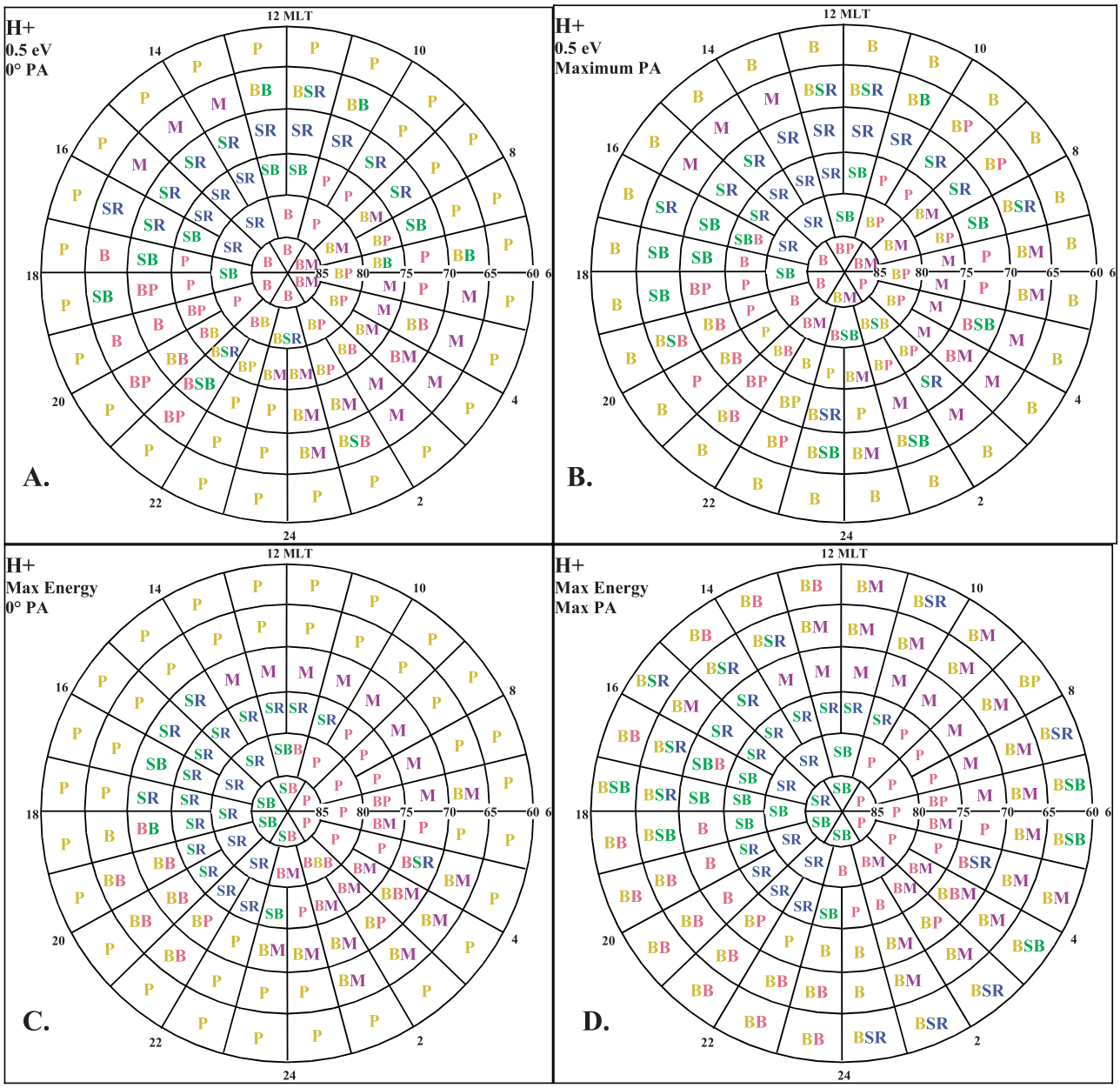

Figure 15. Results of model trajectories run for polar wind H^+ ions for each location as specified by Figure 8.

sheet and ring current trajectories typically originate in the high-latitude dusk sector which is a westward shift in origin from the low-energy polar wind in Figures 15a and 15b.

[48] Finally, trajectories for polar wind ions initiated at the maximum energy and pitch angle are show in Figure 15d. Some distinctly different patterns are seen for these ions. Most noticeably, a number of ions starting at very low latitudes (<65 degrees invariant latitude) make it out to the plasma sheet after some low-energy bouncing between hemispheres. Other patterns are similar to Figure 15c for ions starting at higher latitudes.

[49] Overall, cold bouncing and convecting ions originate from high pitch angle low-latitude polar wind and polar

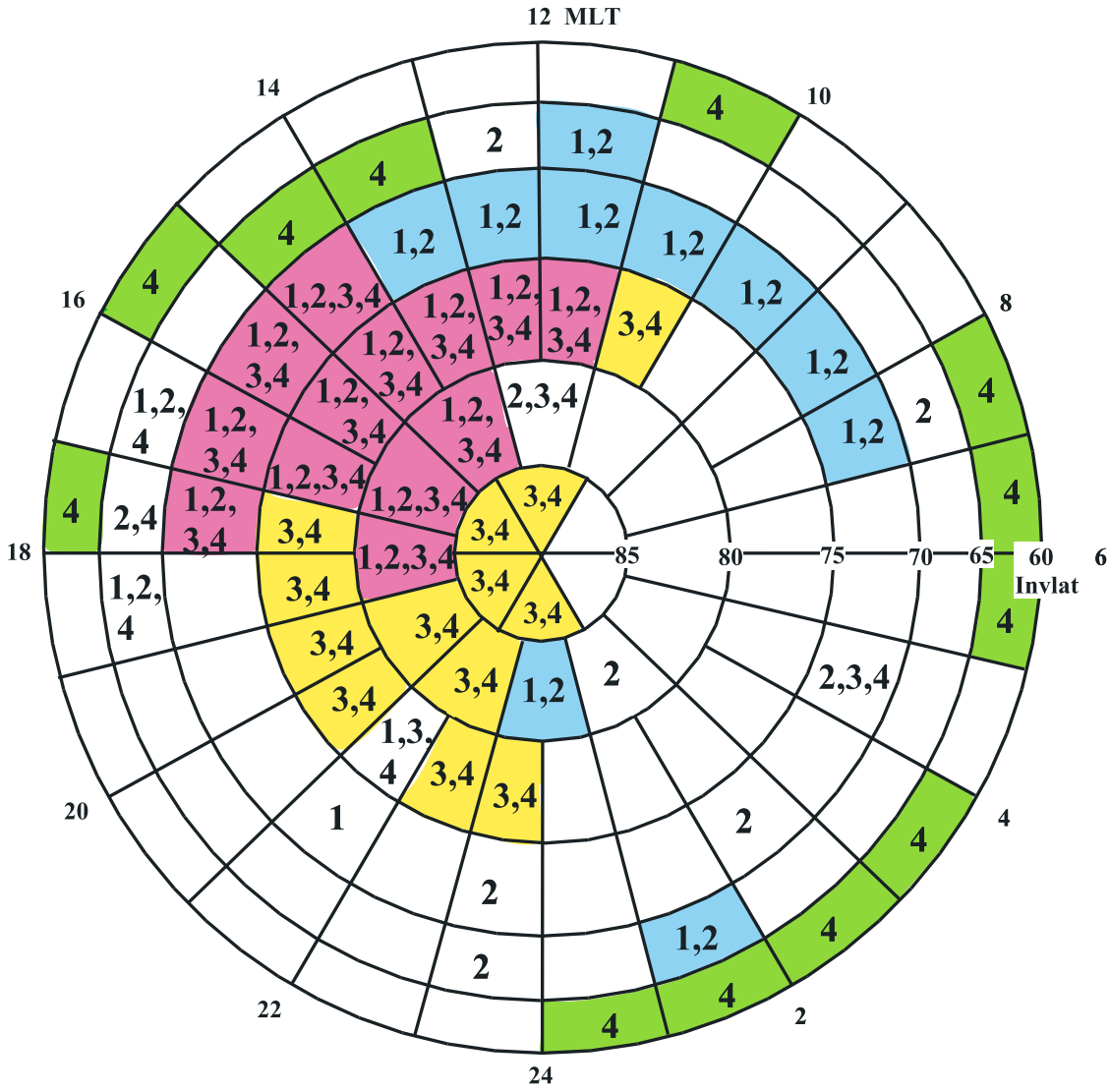

Figure 16. Map of source locations for polar wind ions that contribute to the plasma sheet. Different colors represent specific energy/pitch angle source regions discussed in the text.

wind of a range of pitch angles from nightside through morning local times. Warm bouncing and convecting ions have a persistent source in the evening sector below 75 degrees invariant latitude. They also come from low-energy polar wind exiting at high latitudes directly over the polar cap. Some originate at various latitudes in the morning sector and they often follow a period of cold bouncing behavior. High-energy (>0.5 keV) bouncing ions originate from scattered locations and almost always follow a period of ion residence in the plasma sheet (typically less than 4 hours).

[50] As shown above, the outcome of a polar wind ion was clearly dependent on its initial pitch angle. Varying the pitch angle from the minimum to maximum values could determine fate of the ion, for example, whether it immediately precipitated or continued reflecting between hemispheres. However, pitch angle differences in outflowing polar wind also demonstrated more subtle effects in the

model trajectories. In general, ions with larger pitch angles take longer to travel out across the polar cap and thus have the opportunity to drift more earthward in the lobes than a perfectly field-aligned ion would.

[51] Using Figure 15, we can find the total source region for polar wind H^+ ions that eventually contribute to the energized plasma sheet. Figure 16 illustrates this total source region and shows which ions have access to the plasma sheet. The reader should note that this figure does not yet take into account the source intensity at each location. Regions which act as a plasma sheet source are mainly concentrated in the afternoon and high-latitude evening sectors with scattered low-latitude sources. It is significant to note that there is no overall tendency of either an ion's energy or pitch angle to influence its likelihood of joining the plasma sheet. Instead, each region in local time and latitude has its own conditions for polar wind to feed into the plasma sheet. At invariant latitudes less than about 65 degrees, only maximum energy, maximum pitch angle ions reach the plasma sheet (area shown in light green). In the high-latitude evening sector, higher-energy ions contribute to the plasma sheet regardless of their initial pitch angles (area shown in yellow). Contrasting this region is a band between 70° and 75° invariant latitude, stretching from 7 to 14 magnetic local time, that favors low-energy ions (area shown in light blue). The entire spectrum of polar wind H^+ ions flowing out from the afternoon sector between 70° and 85° invariant latitude is a significant source for the plasma sheet (area shown in pink). It is clear from Figure 16 that a considerable portion of the total polar wind source region at 5000 km is capable of contributing ions to the magnetotail.

8. Polar Wind He^+ Trajectories

[52] Heavier He^+ ions have significantly different trajectories than the H^+ ions described above. Typical polar wind energies for helium are insufficient to accelerate the ions beyond the hemisphere in which they originate. Numerous measurements showed outflow velocities of helium in the polar wind at only a few km/s near 5000 km altitude [e.g., *Chandler et al.*, 1991; *Abe et al.*, 1993]. This translates to less than half an eV in energy for polar wind He^+ ions.

[53] When He^+ ions were initiated with higher energies near 3 eV (approximately equal to the escape speed), the model trajectories showed helium was able to escape the hemisphere of origin. These ions most frequently exhibited a low-energy, convection-dominated ''bouncing'' as described above with H^+ ions. Occasionally a helium ion would bounce out to the magnetotail and join the energetic plasma sheet and ring current or exit the magnetosphere through the magnetosheath.

9. Variations With Magnetic Activity

[54] Since the TIDE data used for determining input parameters for trajectories (see Figure 8) were gathered near solar minimum, magnetic activity was quiet to moderate throughout the survey. All of the above trajectories were modeled for both quiet and moderate cases using *Kp* values of 2 and 4, respectively, by changing the magnetic and electric field components of the model. There was very little variation in the qualitative aspects of the trajectories for these two cases, particularly in regards to how the trajectories were classified. Figure 17 shows an overlay of trajectories for quiet ($Kp = 2$) and moderate ($Kp = 4$) magnetic activity with otherwise identical initial conditions. Although both trajectories pass through similar regions of geospace and reach similar energies, the ion in the quiet magnetosphere travels several R_E farther into the magnetotail. This is due to the fact that as magnetic activity increases, the convection electric fields increase and particles quickly enter the neutral sheet without drifting as far downtail.

[55] For calculating the total density of plasma sheet ions of polar wind origin, an accurate knowledge of the size and shape of the plasma sheet is important. The model trajectories allow a semiempirical estimation of the physical boundaries of the plasma sheet created by polar wind ions for times of both quiet and moderate magnetic activity. Figure 18 shows the resulting plasma sheet location created by overlaying all trajectories where ions traverse the magnetotail with energies greater than 500 eV and less than 5 keV. The top two panels represent the plasma sheet dimensions for moderate magnetic activity, while the lower two panels represent the larger, quiet-time plasma sheet.

10. Cleft Ion Fountain Trajectories

[56] The cleft ion fountain (CIF) is another important source of outflowing ionospheric material [*Lockwood et al.*, 1985a; *Waite et al.*, 1986; *Pollock et al.*, 1990; *Yau and Andre*, 1997]. Sample trajectories were modeled for H^+, He^+, and O^+ ions initiated from a region spanning 8 to 16 hours in magnetic local time and 70 to 80 degrees in invariant latitude. This corresponds roughly to the source region for CIF ions in the cusp/cleft [*Kremser and Lundin*, 1990]. Other CIF characteristics were approximated by initializing each ion at 5000 km altitude with an energy ranging from 10 to 20 eV and a pitch angle of 45 degrees.

[57] Figure 19 shows the typical destinations for modeled ions exiting the CIF source region. The format is similar to that of Figure 15 with the exception that color indicates species rather than energy. It is clear that most of the CIF hydrogen is too energetic to remain in the magnetosphere and is quickly swept out into magnetosheath. Much of the helium initialized at lower latitudes also escapes, though higher-latitude outflows succeed in joining the plasma sheet. Of these three CIF ions, oxygen most easily contributes to the plasma sheet as well as the ring current.

[58] Figure 20 is an overlay of CIF trajectories for H^+, He^+, and O^+ ions. The initial local times are similar, ranging from 8.5 to 10.5 hours. All other initial conditions for the three ions are identical. All three ions exhibit similar qualitative behavior, traveling upward through the lobes to the plasma sheet, where they are energized and sent earthward to join the ring current. However, a striking mass-separation effect is also seen in this figure. The H^+, He^+, and O^+ ions reach maximum geocentric distances in the tail of 65 R_E, 43 R_E, and 25 R_E, respectively. It is also interesting to compare the energy profiles of the three ions. Heavier ions decrease in energy quickly at first but then receive a larger centrifugal ''kick'' over the pole. The heavier ions also receive a greater energy increase upon first entering the

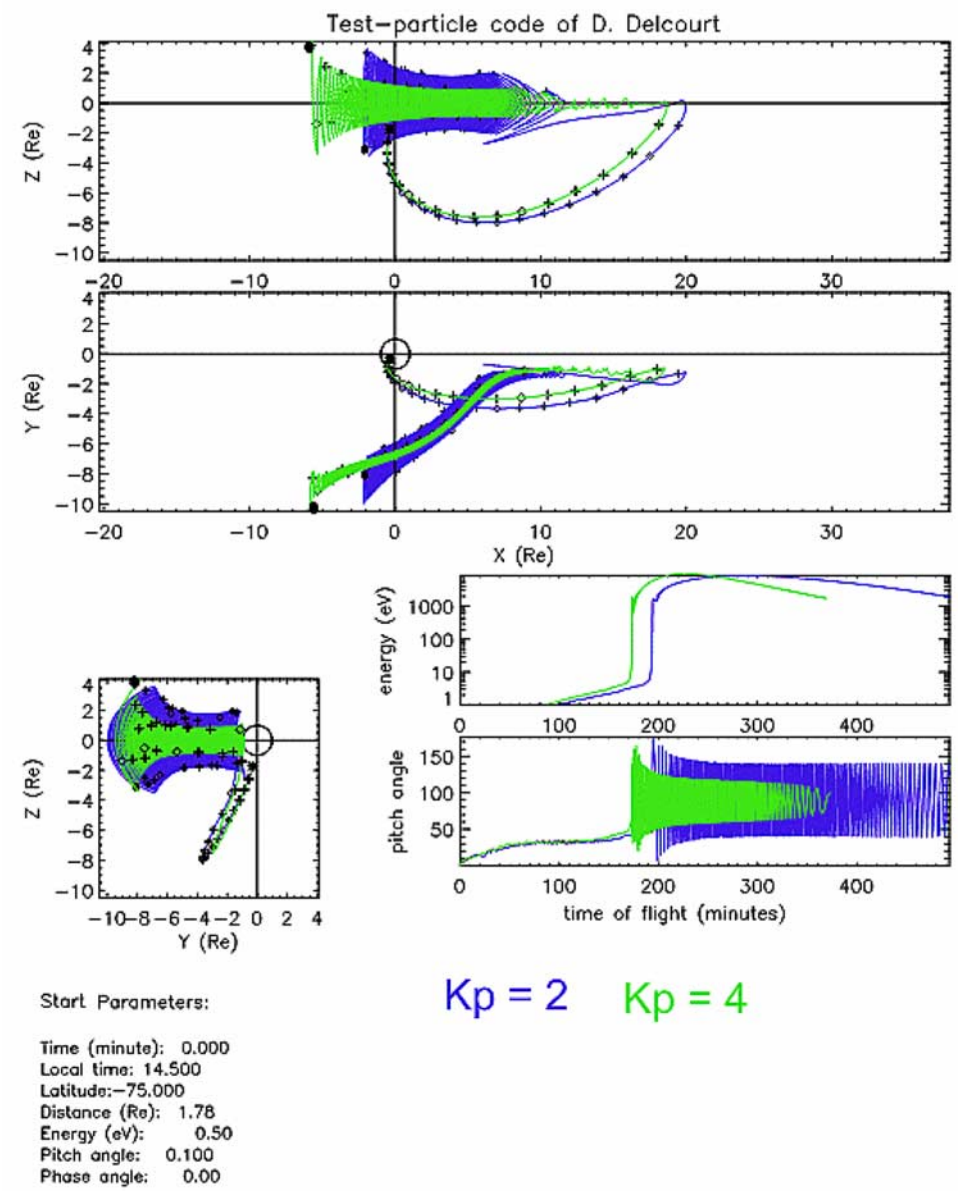

Figure 17. Sample overlay of polar wind ion trajectories for moderately active and quiet magnetic conditions.

plasma sheet, though all three species reach a similar maximum energy in the ring current.

[59] The similarities between trajectories for ions of CIF and polar wind origin suggest that ions from these sources may be indistinguishable when observed in the plasma sheet or other regions through out the magnetosphere.

11. Auroral Ion Trajectories

[60] A number of model trajectories were run for H^+ and O^+ auroral outflows. These ions were initiated at 5000 km altitude from within regions of typical auroral latitudes and local times. Ions were given an initial energy of 500 eV and pitch angles ranging from 0 to 45 degrees. Nearly all of these ions either immediately precipitated in the conjugate ionosphere or exhibited a drifting and "bouncing" behavior. The energies of these ions rarely exceeded a few keV. The high initial velocity of these ions apparently prevents them from drifting through the cross-tail potential enough to experience the rapid increases in energy that were seen in the polar wind trajectories. After a few bounces, the auroral ions would often drift into the magnetosheath or start to lose energy and become convection-dominated, bouncing ions. Although these ions contribute to the inner plasma sheet, their average residence time is relatively brief, and they fail to receive the dramatic increase in energy that CIF and polar wind ions receive. It also appears from the ion trajectories that auroral ions do not contribute significantly to the ring current population.

12. Comparison of Model Results to Observations

[61] For more detailed observational characteristics of the plasma sheet, it is important to refer to several previous studies which utilized spacecraft with orbits reaching farther downtail. *Baumjohann et al.* [1989] reported ion temper-

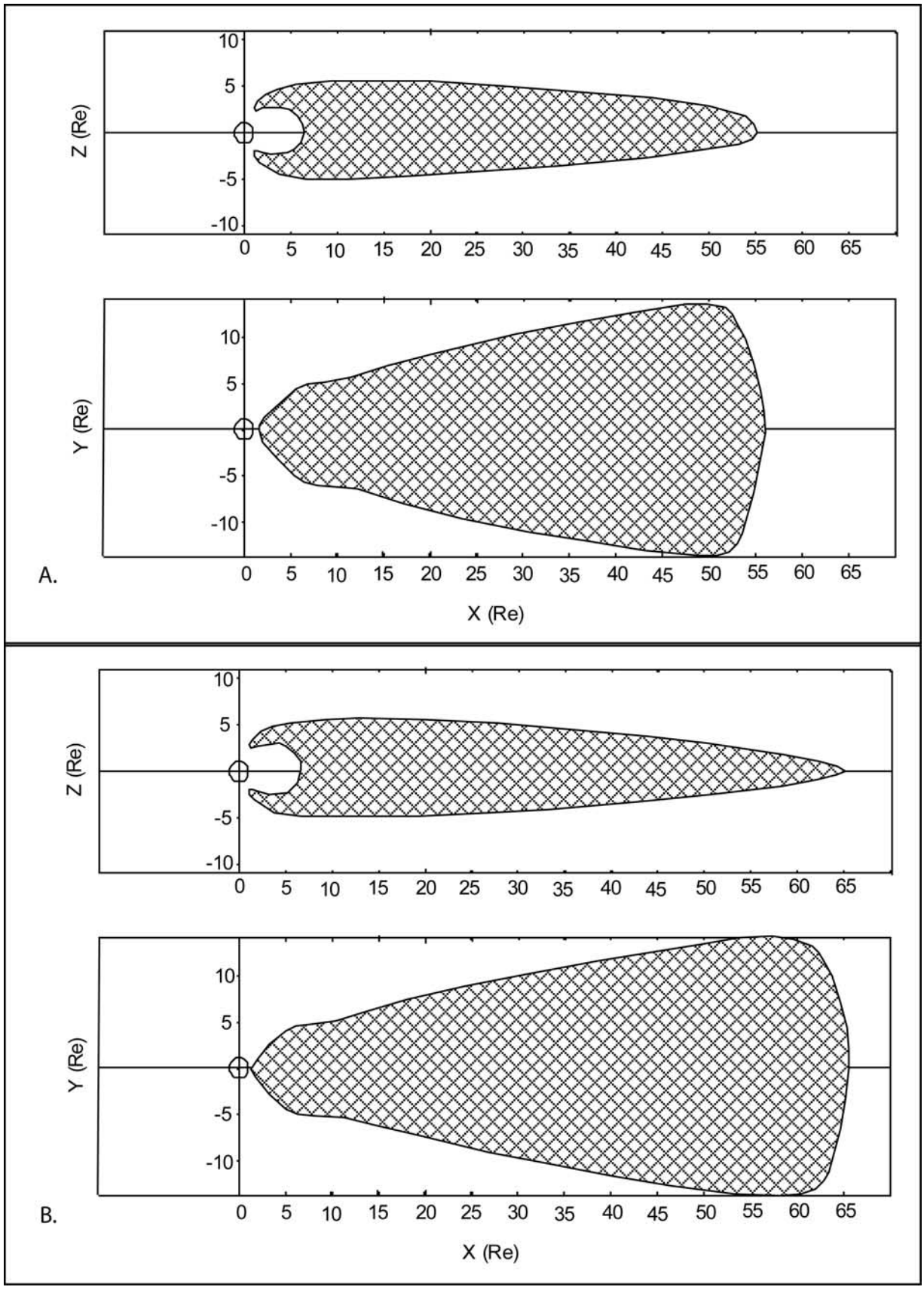

Figure 18. Semiempirical size and shape of the energetic (greater than 0.5 keV) plasma sheet for (a) moderately active and (b) quiet magnetic conditions.

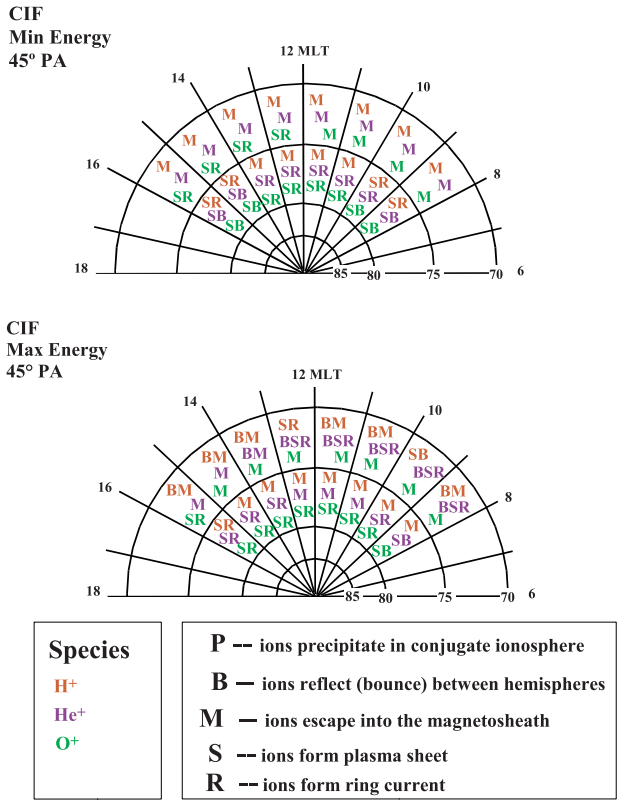

Figure 19. Results of model trajectories run for (top) 10 eV and (bottom) 20 eV CIF ions flowing out of the cusp/cleft region at 5000 km altitude.

atures averaging about 2 to 4 keV, decreasing away from the central plasma sheet from a geocentric distance of 9 R_E to almost 20 R_E.

[62] *Huang and Frank* [1994] reported ion temperatures in the plasma sheet ranging from about 2.5 keV to 6 keV. They also clearly observed higher ion temperatures on the duskside than on the dawnside of the plasma sheet. Bulk velocities were mainly westward on the duskside, while a combination of westward and eastward flows were present on dawnside. Most of the flows were directed earthward in agreement with the observations of *Baumjohann et al.* [1989].

[63] *Lennartsson* [2001] reported plasma sheet measurements of mass resolved ions in the 0.1 keV to 16 keV energy range earthward of about 23 R_E. H^+ mean energies (thermal plus drift energy) ranged from about 500 eV to over 6 keV, increasing with magnetic activity. Although ion flows were predominantly earthward, significant tailward flows of all ion species were also seen, particularly at higher latitudes. Ion energies and drift speeds were greater for earthward flows than tailward flows. Overall, considerable similarity in energy, flow velocity, and location was observed for all tailward drifting ions in the boundary between the plasma sheet and tail lobes, suggesting a common terrestrial source for these ions.

[64] *Nishida* [1999] reported Geotail measurements of cold dense ion distributions in the tail lobes as far as 150 R_E downtail from the Earth. These were interpreted to be a mixture of ionospheric material and decelerated solar wind. *Seki et al.* [2003] examined data from when the Geotail spacecraft entered the shadow of the Earth and the spacecraft potential was greatly reduced. During these times, significant populations of cold ions (tens of eV) were observed in the plasma sheet out to geocentric distances of 19 R_E.

[65] A new investigation of Cluster data by *Sauvaud et al.* [2004] examines several case studies that suggest low-energy terrestrial ions are filling the tail lobes and entering the plasma sheet. Low-energy plasma is commonly observed in the Cluster data throughout the magnetotail, particularly in places where E × B and curvature drifts allow cold ions to overcome spacecraft charging effects. Energy dispersed structures of H^+, He^+, and O^+ are seen in the plasma sheet with the lowest-energy ions seen flowing tailward. Sudden enhancements in ion energy observed by Cluster also point toward local acceleration of colder ions in the plasma sheet. During magnetically active times, single event injections of terrestrial O^+ are estimated to be responsible for up to 80% of the plasma sheet density.

[66] The model trajectory results appear to correlate very well with the basic plasma sheet characteristics described above. The trajectories demonstrate how the source of plasma for the high-energy plasma sheet and ring current can be the ions that are known to flow out of the ionosphere. Although it has been suggested that the predominance of earthward flows indicate that solar wind plasma must be the major source for the plasma sheet [*Lennartsson*, 2001], this view does not take into account the cold ions in the lobes which are invisible to the ISEE 1 Plasma Composition Experiment due to spacecraft charging and which turn earthward at much greater distances than 23 R_E. The model trajectories of ionospheric ions suggest that they would create the earthward flows seen by plasma sheet observational surveys. The most recent reports of cold ions in the magnetotail from Geotail and Cluster appear to support this view.

[67] The typical observed energies and flow velocities appear to match those predicted for a plasma sheet formed by ionospheric material. Modeled trajectories of ions in the 0.5 to ~5 keV range (typical of observed plasma sheet energies) were shown in the previous section to form a region surprisingly similar to the classical plasma sheet (Figure 18). The trajectories predict that ions will mainly flow earthward in the central plasma sheet and tailward at higher latitudes in agreement with observation. The tendency for inner plasma sheet ions on the duskside to flow westward and ions on the dawnside to have a mix of eastward and westward flows [*Huang and Frank*, 1994] can clearly be seen in the model ion trajectories as well. This is simply explained by the fact that sunward convection competes with curvature drifts on the dawnside such that more energetic ions (greater than about 3 keV) drift west to join the ring current while less energetic ions are pushed eastward by convection. On the duskside, however, both drifts are directed westward, consistent with observations.

13. Densities and Energies of Ionospheric Ions in the Magnetotail

[68] All of the instruments mentioned in the previous section with the exception of those on board the Cluster

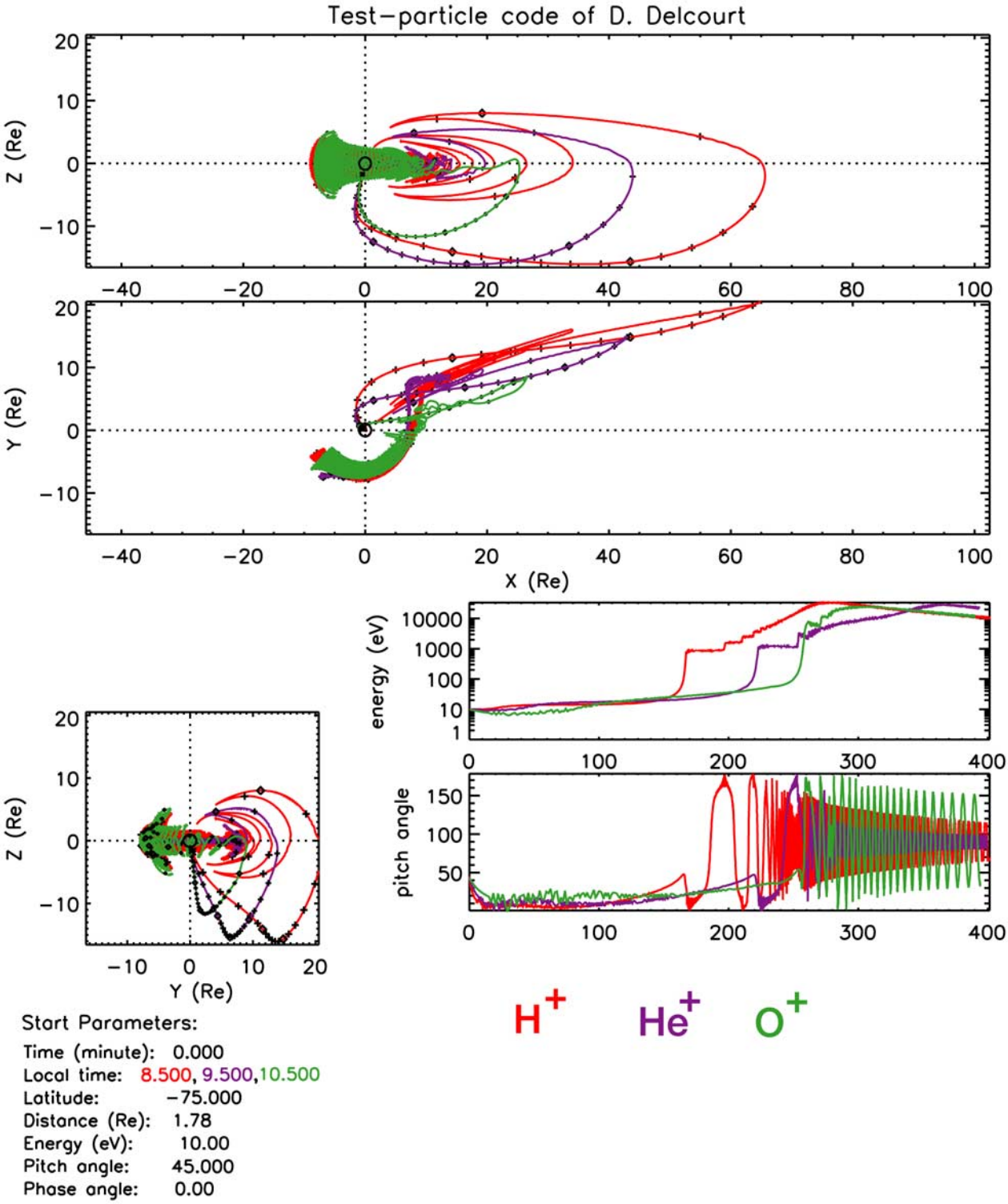

Figure 20. An overlay of cleft ion fountain trajectories for three different species that exit the cleft at similar local times.

spacecraft were unable to actively counter spacecraft charging effects and thus were unlikely to detect large populations of cold ions that may exist in the tail lobes and plasma sheet. However, in the central plasma sheet, the model trajectories suggest that cold ions will be accelerated up to observable energies. Therefore modeled ion outflow fluxes can be directly compared with observed plasma sheet densities.

[69] Polar wind, cleft ion fountain, and auroral outflows are considered to be the three major contributors of ionospheric plasma to the magnetotail. All three sources are quantified and totaled below to compare with the overall

Table 2. Calculated Ion Inflow and Content Provided to the Plasma Sheet From Various Ionospheric Sources

			Source Area at 5000 km Altitude, $\times 10^{17}$ cm^2	Upward Flux of Ions Entering the Plasma Sheet,[a] $\times 10^8$ ions cm^{-2} s^{-1}	Total Rate of Inflow to Plasma Sheet, $\times 10^{25}$ ions s^{-1}	Average Plasma Sheet Ion Residence Time, s	Total Number of Ions in the Plasma Sheet, $\times 10^{28}$
Polar Wind (H^+)	Nightside	Quiet	0.976	0.15–2.4	0.14–2.4	1920	0.28–4.6
		Active		0.30–4.8	0.29–4.8	1340	0.38–6.4
	Dayside	Quiet	4.70	0.15–2.4	0.69–12	1920	1.3–22
		Active		0.30–4.8	1.4–23	1340	1.9–31
Cleft Ion Fountain	O^+	Quiet	1.47	0.14–2.2	0.20–3.2	1350	0.27–4.3
		Active		1.1–8.2	1.6–12	940	1.5–11
	He^+	Quiet	1.28	0.014–0.22	0.017–0.28	1650	0.029–0.46
		Active		0.11–0.82	0.14–1.0	1150	0.16–1.2
	H^+	Quiet	0.765	0.045–0.73	0.035–0.56	2100	0.073–1.2
		Active		0.36–2.7	0.28–2.1	1470	0.41–3.1
Aurora	O^+	Quiet			1.2–7.9	840	1.0–6.6
		Active			2.4–16	600	1.4 – 9.5
	H^+	Quiet			2.1–3.4	1200	2.5–4.1
		Active			4.2–6.8	1000	4.2–6.8

[a]Upward fluxes adjusted to 5000 km altitude.

observed plasma sheet densities. This will give direct information regarding the ability of the ionosphere to supply the magnetosphere with plasma.

13.1. Polar Wind Contribution

[70] TIDE measurements were used as much as possible to determine polar wind flux values. For magnetically quiet times, a range of corrected fluxes from the TIDE survey was used, with upper and lower bounding limits of one logarithmic standard deviation from the average value of 6.0×10^7 ions cm^{-2} s^{-1}. As explained above, these fluxes correspond to measurements acquired during solar minimum, with moderate to low magnetic activity. Polar wind fluxes are theoretically expected to increase by about a factor of two during magnetically active times [*Su et al.*, 1998b; *Schunk and Sojka*, 1997]. Thus the range of fluxes used in Table 2 for magnetically active condition is twice the quiet time values.

[71] The source area for polar wind ions feeding the plasma sheet was calculated using the results of trajectory mapping as shown in Figures 15 and 16. Plasma sheet ions were defined as those ions with energies between 0.5 and 5 keV in the tail. The source area was calculated for an altitude of 5000 km in accordance with the TIDE observations and doubled to account for both the northern and southern ionospheric sources. From certain sectors of the topside ionosphere, only the portion of the ion outflow distribution with the proper combination of pitch angle and energy contributed to the plasma sheet. This was taken into account in calculating the polar wind outflow by reducing the relevant sector area appropriately (equivalently, fluxes could have been individually adjusted for each sector). Since the observed fluxes did not vary appreciably over the range of energies and pitch angles that were modeled, each set of initial conditions (minimum energy–minimum pitch angle, minimum energy–maximum pitch angle, maximum energy–minimum pitch angle, and maximum energy–maximum pitch angle) was assumed to represent one fourth of the overall flux. The adjusted source areas were divided into dayside (0300 to 2100 MLT) and nightside (2100 to 0300 MLT) regions and multiplied by the same range of fluxes to give the total rate of ion inflow to the plasma sheet (third column in Table 2). We have used the measured fluxes acquired during winter hemisphere high zenith angle conditions for both the day and night source areas even though the true dayside fluxes could be significantly larger.

[72] The residence time for ions within the plasma sheet was calculated by simply timing the portion of the trajectory during which ions remained at plasma sheet energies (0.5 to 5 keV) and locations (determined by Figure 18). Polar wind ion residence times ranged from about 20 min to over an hour, with average values near 32 min for a low *Kp* magnetosphere and 22.3 min for a more active magnetosphere. The number of polar wind ions in the plasma sheet at any given time was then found by multiplying the residence times by the corresponding ion inflow rates.

13.2. CIF and Auroral Zone Contribution

[73] In calculating the plasma sheet contribution due to cleft ion fountain (CIF) ions, the source area was determined with the same method used above for polar wind. Trajectory results (see Figure 19) were examined to create an adjusted source area at 5000 km altitude. A range of fluxes for H^+, O^+, and He^+ ions was determined from DE 1/RIMS [*Pollock et al.*, 1990] and Akebono [*Cully et al.*, 2003a] measurements and adjusted to 5000 km altitude. The third column in Table 2 shows the integrated fluxes of CIF ions that reach the plasma sheet. Average CIF ion residence times, as determined from model ion trajectories, are shown in the next column of the table. Heavier ions tended to have shorter "lifetimes" in the plasma sheet on average and to remain closer to the earth than lighter ions due to the so-called "geomagnetic mass spectrometer" effect [*Lockwood et al.*, 1985b] as demonstrated in Figure 20.

[74] Since auroral outflows can be highly variable, a range of typically reported average outflow rates [*Peterson et al.*, 2001; *Abe et al.*, 1996; *Yau et al.*, 1988] have been used in place of a fixed source area or flux value. This assumes that all auroral outflow contributes to the plasma sheet, which is expected due to the fact that auroral latitudes map directly into the central plasma sheet. The highly

Table 3. Calculated Density of Plasma Sheet Resulting Solely From Ionospheric Sources

		Total Number of Ions in Plasma Sheet, $\times 10^{29}$ ions	Plasma Sheet Volume, $\times 10^{29}$ cm^3	Calculated Plasma Sheet Density, ions cm^{-3}	Observed Plasma Sheet Density, ions cm^{-3}	Reference
H^+	Quiet	0.42–3.2	13.0	0.032–0.24	0.11–0.51	[*Lennartsson*, 2001]
	Active	0.68–4.7	9.0	0.076–0.52	0.09–0.36	
He^+	Quiet	0.0029–0.046	13.0	0.00022–0.0035	Roughly 1% to 2% of H^+	[*Lennartsson*, 2001, Figure 6]
	Active	0.016–0.12	9.0	0.0018–0.013		
O^+	Quiet	0.13–1.1	13.0	0.010–0.084	0.024–0.073	[*Lennartsson*, 2001]
	Active	0.29–2.1	9.0	0.033–0.23	0.051–0.066	
Total	Quiet	0.55–4.3	13.0	0.04–0.33	0.2–0.43	[*Haung and Frank*, 1994]
	Active	1.0–6.9	9.0	0.11–0.77	0.12–0.44	

energetic nature of auroral outflows keeps them from experiencing significant convective drift before they reach the central plasma sheet and allows them to be easily seen at plasma sheet energies. Model trajectories were used as before to estimate the average residence time for auroral ions. However, since many auroral trajectories made multiple passes through the plasma sheet, residence times for these ions are estimated with less accuracy than for the polar wind or CIF sources. Another source of uncertainty for auroral trajectories is that they are often believed to be associated with parallel electric fields; such fields were not included in the model trajectory code.

14. Plasma Sheet Densities

[75] By approximating the semiempirical plasma sheet from Figure 18 as a geometric wedge, estimates of 9×10^{29} cm^3 and 1.3×10^{30} cm^3 were made for the plasma sheet volume under moderate and quiet conditions, respectively. The volumes were used together with the results from Table 2 to calculate the expected total ion density, as well as the overall H^+, O^+, and He^+ densities in the plasma sheet resulting from all terrestrial sources. These calculated densities are shown in Table 3.

[76] Using AMPTE/IRM, *Baumjohann et al.* [1989] found overall plasma densities between 0.1 and 0.6 cm^{-3} with average values near 0.4 cm^{-3} and 0.3 cm^{-3} for data gathered earthward and tailward of 14 R_E, respectively. Average densities for the entire plasma sheet equatorward of 20 R_E ranged from 0.25 to 0.45 cm^{-3} during low *AE* conditions and from 0.14 to 0.44 cm^{-3} during high *AE* conditions.

[77] *Huang and Frank* [1994] measured average densities from the ISEE 1 Lepedea plasma analyzer equatorward of 23 R_E. During low *AE* conditions, densities ranged from about 0.2 to 0.43 cm^{-3} with an average value of 0.28 cm^{-3}. High *AE* indexes corresponded to plasma sheet densities ranging from 0.12 to 0.44 cm^{-3} with an average value near 0.25 cm^{-3}.

[78] *Lennartsson* [2001] used observations from the Plasma Composition Experiment on ISEE 1 to calculate mass resolved densities for the central plasma sheet and the plasma sheet boundary under northward and southward IMF conditions. Central plasma sheet densities averaged as high as 0.51 cm^{-3} for H^+ and 0.073 cm^{-3} for O^+ under northward IMF conditions. When the IMF was directed southward, H^+ average densities up to 0.36 cm^{-3} and O^+ average densities near 0.065 cm^{-3} were observed in the central plasma sheet. At the boundary between the lobes and the plasma sheet, H^+ averages were as low as 0.11 cm^{-3} during northward IMF and 0.092 cm^{-3} during southward IMF. O^+ densities in this boundary region fell to 0.024 cm^{-3} and 0.051 cm^{-3} for north and south IMF, respectively. He^+ densities were not calculated separately by *Lennartsson* [2001] but were typically detected on the order of 1 to 2 percent of the H^+ density [see *Lennartsson*, 2001, Figure 6]. All of these observational densities are summarized on Table 3 in comparison with the calculated values for plasma sheet densities.

[79] The calculated densities actually represent large-scale average densities over the entire plasma sheet (out to 65 R_E), which are expected to be somewhat lower than the observations with which they are being compared. The pressure gradient in the tail means that higher densities are found closer to the Earth [*Baumjohann et al.*, 1989]. Since the ISSE 1 and AMPTE measurements were relatively close to Earth (less than 23 R_E), they should represent higher densities than the average density throughout the entire plasma sheet.

[80] Interestingly, all of the observational values overlap significantly with the range of calculated densities for the plasma sheet. This would imply that little if any external source of plasma is needed in addition to the ionospheric source in order to account for current observations. The only exception to this is the significant observed population of He^{++} ions in the plasma sheet, whose source has not been considered here.

15. Tail Lobe Densities

[81] The same procedure outlined above was used to calculate ionospheric ion outflow into the tail lobes. Slightly different source areas were used since certain ions were included that traversed the lobes but exited the magnetosheath instead of entering the plasma sheet. Tail lobe ion residence times were also calculated from model trajectories in the same way that the plasma sheet residence times were obtained. Auroral ions were excluded as a source since these ions rarely traveled into the distant lobe regions according to model trajectories. The resulting tail lobe inflow rates and ion content are shown in Table 4.

[82] The tail lobe volume was calculated by subtracting the appropriate plasma sheet volume (determined above) from a cylindrical volume with a length equal to the length of the plasma sheet and a diameter equal to the width of the plasma sheet. The ion content from Table 4 was then

Table 4. Calculated Ion Inflow and Content Provided to the Tail Lobes From Various Ionospheric Sources

			Source Area at 5000 km Altitude, $\times 10^{17}$ cm^2	Total Rate of Inflow to the Tail Lobe, $\times 10^{25}$ ions s^{-1}	Average Tail Lobe Ion Residence Time, s	Total Number of Ions in the Tail Lobe, $\times 10^{28}$
Polar Wind (H^+)	Nightside	Quiet	2.29	0.34–5.6	10080	3.4–56
		Active		0.67–11	9800	6.6–110
	Dayside	Quiet	4.82	0.71–12	12600	8.9–150
		Active		1.4–24	11200	16–260
Cleft Ion Fountain	O^+	Quiet	1.60	0.22–3.5	6600	1.4–23
		Active		1.8–13	6250	11–82
	He^+	Quiet	1.53	0.021–0.33	5700	0.12–1.9
		Active		0.17–1.3	5480	0.91–6.9
	H^+	Quiet	1.40	0.064–1.0	4800	0.31–4.9
		Active		0.51–3.8	4520	2.3–17

divided by the tail lobe volume to yield the density estimates which are shown in Table 5. Observational measurements of the colder ionospheric ions suspected to permeate the tail lobes are problematic due to spacecraft charging effects. Thus no observed densities are given in Table 5 to compare with the calculated values. Measurements of *Eastman et al.* [1985] report tail lobe densities less than 0.1 cm^{-3}. The comparatively large tail lobe densities calculated in Table 5 suggest that significant populations of cold ions with energies of 10's of eV or less may be continuously present in the distant lobes.

16. Summary and Conclusions

[83] In the quest to answer questions of magnetospheric plasma origins, several new and exciting insights have been obtained regarding the structure and dynamics of the magnetosphere. Our results suggest that the ionosphere appears to be fully capable of supplying the magnetosphere with plasma at the appropriate range of energies and densities needed to fit observations with the exception of the well documented He^{++} component. The acceleration processes necessary for ionospheric ion entry into the plasma sheet do not require any complex theoretical approach to be explained but rather naturally arise from conservation of the first adiabatic invariant and ion drifts through known magnetic and electric fields found within the magnetosphere. The work here strongly argues for the existence of cold populations (<50 eV) of ionospheric material throughout much of the outer magnetosphere that would be difficult, if not impossible, to detect with current orbiting particle instruments because of positive spacecraft potentials. Thus renewed efforts are needed to address the implications of the ionosphere as a source of plasma for the magnetosphere.

[84] Several new steps have been taken in this work that make it a significant improvement on previous research in this area. A detailed statistical analysis of pitch angle and energy distributions of polar wind (<3.5 eV) outflows was performed using TIDE data. A bi-Maxwellian fitting technique using updated values of spacecraft potential have provided new estimates of polar wind fluxes that are substantially higher than previously published values [*Su et al.*, 1998a]. Using the results of the observational study, thousands of model trajectories were calculated that traced ion paths from all three major terrestrial outflow sources (polar wind, CIF, and auroral zone). The information collected from the model trajectories was compared both qualitatively and quantitatively with numerous observational studies from satellite instruments in a variety of magnetospheric locations. In addition to explaining many basic observed characteristics of the magnetosphere such as energy and density, the information compiled from the model trajectories has also suggested several predictions regarding expected observations from improved future instrumentation.

[85] All of the details mentioned above make this work a significant addition to previous work by *Chappell et al.* [1987] and *Cully et al.* [2003b] to understand the ionosphere as a source of magnetospheric plasma. A specific source function was used as input to a detailed magnetospheric model. Energization of polar wind ions from a few eV to tens of eV over the polar caps and to several keV in the plasma sheet was explained rather than assumed. The shape and size of the plasma sheet were obtained from the ion trajectories, which were dependent on model electric

Table 5. Calculated Tail Lobe Density Resulting Solely From Ionospheric Sources

		Total Number of Ions in Tail Lobe, $\times 10^{29}$ ions	Tail Lobe Volume, $\times 10^{30}$ cm^3	Calculated Tail Lobe Density, ions cm^{-3}
H^+	Quiet	1.3–21	13.0	0.010–0.16
	Active	2.5–39	5.0	0.050–0.78
He^+	Quiet	0.012–0.19	13.0	0.0001–0.001
	Active	0.091–0.69	5.0	0.0018–0.014
O^+	Quiet	0.14–2.3	13.0	0.0011–0.018
	Active	1.1–8.2	5.0	0.022–0.16
Total	Quiet	1.4–23	13.0	0.011–0.18
	Active	3.7–48	5.0	0.073–0.96

and magnetic fields, rather than determined independently. Numerous other distinctions exist, including the explanation of terrestrial ion entry into the ring current and the formation of eastward convecting double field-aligned flows.

[86] This new research has revealed a number of surprising new challenges to the traditional view of ionospheric outflow, including the following:

[87] 1. There appears to be a sufficient calculated density of ionospheric ions in the plasma sheet to account for observations, with the exception of the well-established He^{++} plasma sheet component. Any solar wind source may actually be very minor compared with the terrestrial source strength. Polar wind appears to be the dominant source for H^+ ions, while O^+ is supplied by the CIF and auroral sources which exhibit more variation with magnetic activity. This explains how oxygen and hydrogen outflow rates can show markedly different dependences on solar wind conditions or magnetic activity [*Cully et al.*, 2003a].

[88] 2. A number of model trajectories terminated with ions leaving the magnetosphere and entering the magnetosheath. While the exact fate of these ions is uncertain, this may imply that significant amounts of terrestrial plasma are continuously lost to the interplanetary medium. Magnetospheric plasma may also necessarily be lost to the interplanetary medium in order to account for the levels of He^{++} that have been documented in the plasma sheet.

[89] 3. Much of the polar wind and cleft ion fountain reach the plasma sheet and are accelerated to typical plasma sheet energies. The basic characteristics (size, shape, energy, flow speeds, composition) of the plasma sheet formed by model ion trajectories are similar to observed plasma sheet characteristics. The model also predicts ring current formation and other magnetospheric populations (with characteristics consistent with observations) being created from ionospheric ions.

[90] 4. Calculations of tail lobe densities indicate that the lobes can be full of cold, less than 50 eV, plasma with densities exceeding 0.5 cm^{-3}, yet invisible to most instruments. Recent data from the Cluster satellite [*Sauvaud et al.*, 2004; *Seki et al.*, 2003] appears to support this prediction.

[91] 5. The initial values of energy and pitch angle for individual polar wind ions appear to have an important effect on the ultimate destination of these ions (Figure 15). Model trajectories indicate that most polar wind He^+ is gravitationally bound, but that cleft ion fountain helium is energetic enough to exit the polar cap. This could explain the relatively small amount of He^+ seen by TIDE at high altitudes [*Su et al.*, 1998a].

[92] 6. Although auroral flows may serve an important role in the energy and dynamics of ionosphere-magnetosphere coupling, particularly during magnetically active times, Table 2 indicates that in certain cases polar wind outflow could well exceed the auroral component when it comes to plasma sheet filling.

[93] 7. The dayside subauroral ionosphere and plasma trough is an unexpected contributor to the plasma sheet and ring current. Low-energy ions equatorward of the cusp receive a proportionally larger centrifugal acceleration due to highly curved field lines convecting across the polar cap. Double field-aligned ions in the dayside plasma trough with energies of a few eV can convect through the polar cusp, polar cap, and tail lobes to gain access to the plasma sheet and ring current.

[94] 8. Most of the H^+ that reaches the plasma sheet enters farther than 20 R_E downtail and immediately turns earthward. Consequently, one would expect terrestrial H^+ to be flowing earthward in the plasma sheet for observations made within 20 R_E. Thus the observations of predominantly earthward flows in the plasma sheet [*Lennartsson*, 2001; *Huang and Frank*, 1994; *Baumjohann et al.*, 1989] do not by any means preclude a dominant ionospheric source. Since model trajectories show species separation in the tail according to mass, earthward flows of O^+ and He^+ should be less prevalent than H^+ flows, though not necessarily uncommon.

[95] 9. Centrifugal acceleration processes over the polar cap [*Cladis*, 1986] are important for energizing O^+, He^+, and H^+ outflow and propelling them out to the magnetotail. Very low-energy polar wind H^+ together with cleft ion fountain H^+, He^+, and O^+ can be accelerated to 10s of eV from simple drift through model electric and magnetic fields without the need for wave-particle interactions or parallel electric fields. Modeled energization from dayside to polar cap seems to increase in proportion to the square root of the ion mass.

[96] 10. The model trajectories effectively illustrate that "regions" of the magnetosphere are places of temporary residence for ions traveling from one location to another. Ions within the magnetotail, plasma sheet, and ring current are always on their way to somewhere else (see Figure 14). Dynamics of the electric and magnetic fields within the magnetosphere are constantly changing the temperatures, flow velocities, and pitch angles of these ions. An ion may circulate through virtually all regions of the magnetosphere before plummeting back into the ionosphere, exiting to join the solar wind, or being recycled back into the magnetosphere.

[97] 11. Detection and quantification of polar wind outflows at altitudes above a few thousand kilometers is severely hampered by spacecraft charging effects. A spacecraft potential of only a few volts can reduce the observed outflow flux by a factor of ten or more. Spacecraft potential measurements available from the Polar electric fields and low-energy electron instruments provided a unique opportunity to reassess the question of polar wind outflow fluxes by statistically correcting TIDE ion measurements to account for suppressed polar wind flux. This independent measurement of spacecraft potential is not available on most currently orbiting satellites. Results of these statistics suggest the presence of a consistent ubiquitous polar wind outflow at all latitudes surveyed (greater than 70 invariant latitude), with average fluxes of approximately 6.0×10^7 ions cm^{-2} s^{-1} (adjusted to 5000 km altitude) during local winter and magnetically quiet conditions.

[98] With the possible exception of the inner radiation belt, it appears that all magnetospheric regions could be supplied by an ionospheric source. Therefore the ionosphere as a source of plasma should be a crucial component of global magnetospheric modeling efforts. Modeling terrestrial ions throughout the magnetosphere has already provided valuable insight into the origins and characteristics of known magnetospheric regions. Using this measured ionospheric source, further study in this direction holds the

promise of answering even more questions regarding the behavior of plasma within the magnetosphere.

[99] **Acknowledgments.** The authors acknowledge support from NASA grant NNG04GB44G entitled "A Study of Ion Outflow as a Source of Plasma for the Magnetosphere."

[100] Arthur Richmond thanks William K. Peterson, Andrew Yau, and another reviewer for their assistance in evaluating this paper.

References

Abe, T., B. A. Whalen, A. W. Yau, R. E. Horita, S. Watanabe, and E. Sagawa (1993), EXOS D (Akebono) suprathermal mass spectrometer observations of the polar wind, *J. Geophys. Res.*, *98*, 11,191.

Abe, T., S. Watanabe, B. A. Whalen, A. W. Yau, and E. Sagawa (1996), Observations of polar wind and thermal ion outflow by Akebono/SMS, *J. Geomagn. Geoelectr.*, *48*, 319.

Arnoldy, R. L. (1993), Transverse ion acceleration by active experiments, in *Auroral Plasma Dynamics*, *Geophys. Monogr. Ser.*, vol. 80, edited by R. L. Lysak, p. 195, AGU, Washington, D. C.

Banks, P. M., and T. E. Holzer (1968), The polar wind, *J. Geophys. Res.*, *73*, 6846.

Barakat, A. R., I. A. Barghouthi, and R. W. Schunk (1995), Double-hump H^+ velocity distribution in the polar wind, *Geophys. Res. Lett.*, *22*, 1857.

Baumjohann, W., G. Paschmann, and C. A. Cattell (1989), Average plasma properties in the central plasma sheet, *J. Geophys. Res.*, *94*, 6597.

Brinton, H. C., J. M. Grebowski, and H. G. Mayr (1971), Altitude variation of ion composition in the mid-latitude trough region: Evidence for upward plasma flow, *J. Geophys. Res.*, *76*, 3738.

Carpenter, D. L. (1963), Whistler evidence of a "knee" in the magnetospheric ionization density profile, *J. Geophys. Res.*, *68*, 1675.

Chandler, M. O., J. H. Waite Jr., and T. E. Moore (1991), Observations of polar ion outflows, *J. Geophys. Res.*, *96*, 1421.

Chappell, C. R., T. E. Moore, and J. H. Waite Jr. (1987), The ionosphere as a fully adequate source of plasma for the Earth's magnetosphere, *J. Geophys. Res.*, *92*, 5896.

Chappell, C. R., B. L. Giles, T. E. Moore, D. C. Delcourt, P. D. Craven, and M. O. Chandler (2000), The adequacy of the ionospheric source in supplying magnetospheric plasma, *J. Atmos. Sol. Terr. Phys.*, *62*, 421.

Cladis, J. B. (1986), Parallel acceleration and transport of ions from polar ionosphere to plasma sheet, *Geophys. Res. Lett.*, *13*, 893.

Cladis, J. B., and W. E. Francis (1992), Distribution in magnetotail of O+ ions from cusp/cleft ionosphere: A possible substorm trigger, *J. Geophys. Res.*, *97*, 123.

Collin, H. L., R. D. Sharp, and E. G. Shelley (1984), The magnitude and composition of the outflow of energetic ions from the ionosphere, *J. Geophys. Res.*, *89*, 2185.

Collin, H. L., W. K. Peterson, J. F. Drake, and A. W. Yau (1988), The helium components of energetic terrestrial ion upflows: Their occurrence, morphology, and intensity, *J. Geophys. Res.*, *93*, 7558.

Cully, C. M., E. F. Donovan, A. W. Yau, and G. G. Arkos (2003a), Akebono/Suprathermal Mass Spectrometer observations of low-energy ion outflow: Dependence on magnetic activity and solar wind conditions, *J. Geophys. Res.*, *108*(A2), 1093, doi:10.1029/2001JA009200.

Cully, C. M., E. F. Donovan, A. W. Yau, and H. J. Opgenoorth (2003b), Supply of thermal ionospheric ions to the central plasma sheet, *J. Geophys. Res.*, *108*(A2), 1092, doi:10.1029/2002JA009457.

Daglis, I. A., and W. I. Axford (1996), Fast ionospheric response to enhanced activity in goespace: Ion feeding of the inner magnetotail, *J. Geophys. Res.*, *101*, 5047.

Delcourt, D. (1985), Circulation des ions ionospheriques suprathermiques dans la magnetosphere terrestre, Ph.D. thesis, Toulouse Univ., Toulouse, France.

Delcourt, D. C., B. L. Giles, C. R. Chappell, and T. E. Moore (1988), Low-energy bouncing ions in the magnetosphere: A three-dimensional numerical study of Dynamics Explorer 1 data, *J. Geophys. Res.*, *93*, 1859.

Delcourt, D. C., C. R. Chappell, T. E. Moore, and J. H. Waite Jr. (1989), A three-dimensional numerical model of ionospheric plasma in the magnetosphere, *J. Geophys. Res.*, *94*, 11,893.

Delcourt, D. C., J. A. Sauvaud, and T. E. Moore (1993), Polar wind ion dynamics in the magnetotail, *J. Geophys. Res.*, *98*, 9155.

Delcourt, D. C., R. F. Martin Jr., J. A. Sauvaud, and T. E. Moore (1995), Centrifugal trapping in the magnetotail, *Ann. Geophys.*, *13*, 242.

Drakou, E., A. W. Yau, and T. Abe (1997), Ion temperature measurements from the Akebono suprathermal mass spectrometer: Application to the polar wind, *J. Geophys. Res.*, *102*, 17,523.

Eastman, T. E., L. A. Frank, and C. Y. Huang (1985), The boundary layers as the primary transport regions of the Earth's magnetotail, *J. Geophys. Res.*, *90*, 9541.

Elphic, R. C., M. F. Thomsen, and J. E. Borovsky (1997), The fate of the outer plasmasphere, *Geophys. Res. Lett.*, *24*, 365.

Ganguli, S. B. (1996), The polar wind, *Rev. Geophys.*, *34*, 311.

Harvey, P., et al. (1995), The electric field instrument on the Polar satellite, *Space Sci. Rev.*, *71*, 583.

Horwitz, J. L., C. W. Ho, H. D. Scarbro, G. R. Wilson, and T. E. Moore (1994), Centrifugal acceleration of the polar wind, *J. Geophys. Res.*, *99*, 15,051.

Huang, C. Y., and L. A. Frank (1994), A statistical survey of the central plasma sheet, *J. Geophys. Res.*, *99*, 83.

Hultqvist, B. (1982), Recent progress in the understanding of the ion composition in the magnetosphere and some major question marks, *Rev. Geophys.*, *20*, 589.

Kivelson, M. G., and H. E. Spence (1988), On the possibility of quasi-static convection in the quiet magnetotail, *Geophys. Res. Lett.*, *15*, 1541.

Kondo, T., B. A. Whalen, A. W. Yau, and W. K. Peterson (1990), Statistical analysis of upflowing ion beam and conic distributions at DE 1 altitudes, *J. Geophys. Res.*, *95*, 12,091.

Kremser, G., and R. Lundin (1990), Average spatial distributions of energetic particles in the midaltitude cusp/cleft region observed by Viking, *J. Geophys. Res.*, *95*, 5753.

Lennartsson, O. W. (2001), Ion composition aspects of magnetotail plasma flows, *J. Geophys. Res.*, *106*, 15,621.

Lockwood, M., J. H. Waite Jr., T. E. Moore, C. R. Chappell, and J. F. E. Johnson (1985a), A new source of suprathermal O^+ ions near the dayside polar cap boundary, *J. Geophys. Res.*, *90*, 4099.

Lockwood, M., T. E. Moore, J. H. Waite Jr., C. R. Chappell, and J. L. Horwitz (1985b), The geomagnetic mass spectrometer - Mass and energy dispersions of ionospheric ion flows into the magnetosphere, *Nature*, *316*, 612.

Lund, E. J., et al. (1998), FAST observations of preferentially accelerated He^+ in association with auroral electromagnetic ion cyclotron waves, *Geophys. Res. Lett.*, *25*, 2049.

Moore, T. E., J. H. Waite Jr., M. Lockwood, and C. R. Chappell (1986), Observations of coherent transverse ion acceleration, in *Ion Acceleration in the Magnetosphere and Ionosphere*, *Geophys. Monogr. Ser.*, vol. 38, edited by T. Chang, p. 50, AGU, Washington, D. C.

Moore, T. E., et al. (1995), The thermal ion dynamics experiment and plasma source instrument, *Space Sci. Rev.*, *71*, 409.

Moore, T. E., W. K. Peterson, C. T. Russell, M. O. Chandler, M. R. Collier, H. L. Collin, P. D. Craven, R. Fitzenreiter, B. L. Giles, and C. J. Pollock (1999), Ionospheric mass ejection in response to a CME, *Geophys. Res. Lett.*, *26*, 2339.

Nagai, T., J. F. E. Johnson, and C. R. Chappell (1983), Low-energy (less than 100 eV) ion pitch angle distributions in the magnetosphere by ISEE 1, *J. Geophys. Res.*, *88*, 6944.

Nishida, A. (1999), Geotail Mission: Accomplishments and prospects, in *Sun-Earth Plasma Connections*, *Geophys. Monogr. Ser.*, vol. 109, edited by J. L. Burch, R. L. Carovillano, and S. K. Antiochos, p. 19, AGU, Washington, D. C.

Peterson, W. K., H. L. Collin, A. W. Yau, and O. W. Lennartsson (2001), Polar/Toroidal Imaging Mass-Angle Spectrograph observations of suprathermal ion outflow during solar minimum conditions, *J. Geophys. Res.*, *106*, 6059.

Pollock, C. J., M. O. Chandler, T. E. Moore, J. H. Waite Jr., C. R. Chappell, and D. A. Gurnett (1990), A survey of upwelling ion event characteristics, *J. Geophys. Res.*, *95*, 18,969.

Sauvaud, J. A., and D. Delcourt (1987), A numerical study of suprathermal ionospheric ion trajectories in three-dimensional electric and magnetic field models, *J. Geophys. Res.*, *92*, 5873.

Sauvaud, J. A., et al. (2004), Case studies of the dynamics of ionospheric ions in the Earth's magnetotail, *J. Geophys. Res.*, *109*, A12213, doi:10.1029/2003JA010333.

Schunk, R. W. (1988), A mathematical model of the middle and high latitude ionosphere, in *Ionospheric Modeling*, edited by J. N. Korenkov, p. 255–303, Springer, New York.

Schunk, R. W., and J. J. Sojka (1997), Global ionosphere-polar wind system during changing magnetic activity, *J. Geophys. Res.*, *102*, 11,625.

Scudder, J., et al. (1995), Hydra-A 3-dimensional electron and ion hot plasma instrument for the Polar spacecraft of the GGS mission, *Space Sci. Rev.*, *71*, 459.

Scudder, J. D., X. Cao, and F. S. Mozer (2000), Photoemission current-spacecraft voltage relation: key to routine quantitative low-energy plasma measurements, *J. Geophys. Res.*, *105*, 21,281.

Seki, K., M. Hirahara, M. Hoshino, T. Terasawa, R. C. Elphic, Y. Saito, T. Mukai, H. Hayakawa, H. Kojima, and H. Matsumoto (2003), Cold ions in the hot plasma sheet of Earth's magnetotail, *Nature*, *422*, 589.

Shelley, E. G., R. G. Johnson, and R. D. Sharp (1972), Satellite observations of energetic heavy ions during a geomagnetic storm, *J. Geophys. Res.*, *77*, 6104.

Sojka, J. J., and R. W. Schunk (1983), A theoretical study of the high-latitude *F* region's response to magnetospheric storm inputs, *J. Geophys. Res.*, *88*, 2112.

Sojka, J. J., R. W. Schunk, J. F. E. Johnson, J. H. Waite, and C. R. Chappell (1983), Characteristics of thermal and suprathermal ions associated with the dayside plasma trough as measured by the Dynamics Explorer Retarding Ion Mass Spectrometer, *J. Geophys. Res.*, *88*, 7895.

Su, Y.-J., J. L. Horwitz, T. E. Moore, B. L. Giles, M. O. Chandler, P. D. Craven, M. Hirahara, and C. J. Pollock (1998a), Polar wind survey with the Thermal Ion Dynamics Experiment/Plasma Source Instrument suite aboard POLAR, *J. Geophys. Res.*, *103*, 29,305.

Su, Y.-J., J. L. Horwitz, G. R. Wilson, P. G. Richards, D. G. Brown, and C. W. Ho (1998b), Self-consistent simulation of the photoelectron-driven polar wind from 120 km to 9 R_E altitude, *J. Geophys. Res.*, *103*, 2279.

Tsyganenko, N. A. (1989), A magnetospheric magnetic field model with a warped tail current sheet, *Planet. Space Sci.*, *37*, 5.

Volland, H. (1979), Semiempirical models of magnetospheric electric fields, in *Quantitative Modeling of Magnetospheric Processes*, *Geophys. Monogr. Ser.*, vol. 21, edited by W. P. Olson, p. 261, AGU, Washington, D. C.

Waite, J. H., Jr., T. E. Moore, M. O. Chandler, M. Lockwood, A. Persoon, and M. Suguira (1986), Ion energization in upwelling ion events, in *Ion Acceleration in the Magnetosphere and Ionosphere*, *Geophys. Monogr. Ser.*, vol. 38, edited by T. S. Chang, p. 61, AGU, Washington, D. C.

Yau, A. W., and M. Andre (1997), Sources of ion outflow in the high latitude ionosphere, *Space Sci. Rev.*, *80*, 1.

Yau, A. W., W. K. Peterson, and E. G. Shelley (1988), Quantitative parametrization of energetic ionospheric ion outflow, in *Modeling Magnetospheric Plasma*, *Geophys. Monogr. Ser.*, vol. 44, edited by T. E. Moore and J. H. Waite, p. 211, AGU, Washington, D. C.

M. O. Chandler, NASA Marshall Space Flight Center, Huntsville, AL 35812, USA.

C. R. Chappell, Vanderbilt University, Nashville, TN 37235, USA.

D. C. Delcourt, CETP, Observatoire de Saint-Maur, CNRS-IPSL, 4, avenue de Neptune, F-94107 Saint Maur des Fossés, France.

B. L. Giles and T. E. Moore, NASA Goddard Space Flight Center, Greenbelt, MD 20771, USA.

M. M. Huddleston, Harpeth Hall School, 3801 Hobbs Road, Nashville, TN 37215, USA. (huddleston@harpethhall.org)